agriculture

MDPI

Article

Investigating Sentinel-1 and Sentinel-2 Data Efficiency in Studying the Temporal Behavior of Wheat Phenological Stages Using Google Earth Engine

Hajar Saad El Imanni [1,*], Abderrazak El Harti [1] and Jonathan Panimboza [2,3]

[1] Team of Remote Sensing and GIS Applied to the Geosciences and the Environment, Faculty of Sciences and Techniques, Beni Mellal 23000, Morocco
[2] Department of Earth and Building Sciences, University of the Armed Forces, ESPE, Sangolqui 171103, Ecuador
[3] Panamerican Center for Geographical Studies and Research, Quito 170136, Ecuador
* Correspondence: hajarsaad94@gmail.com; Tel.: +212-697-488-470

Abstract: Crop monitoring is critical for sustaining agriculture, preserving natural resources, and dealing with the effects of population growth and climate change. The Sentinel missions, Sentinel-1 and Sentinel-2, provide open imagery at a high spatial and temporal resolution. This research aimed (1) to evaluate the temporal profiles derived from Sentinel-1 and Sentinel-2 time series data in deducing the dates of the phenological stages of wheat from germination to the fully mature plant using the Google Earth Engine (GEE) JavaScript interface and (2) to assess the relationship between phenological stages and optical/ SAR remote sensing indices for developing an accurate phenology estimation model of wheat and extrapolate it to the regional scale. Firstly, the temporal profiles derived from Sentinel-1 and Sentinel-2 remote sensing indices were evaluated in terms of deducing the dates of the phenological stages of wheat. Secondly, the remote sensing indices were used to assess their relationship with phenological stages using the linear regression (LR) technique. Thirdly, the best performing optical and radar remote sensing indices were selected for phenological stage prediction. Fourthly, the spatial distribution of wheat in the TIP region was mapped by performing a Random Forest (RF) classification of the fusion of Sentinel-1 and Sentinel 2 images, with an overall accuracy of 95.02%. These results were used to characterize the growth of wheat on the TIP regional scale using the Temporal Normalized Phenology Index (TNPI) and the predicted models. The obtained results revealed that (1) the temporal profiles of the dense time series of Sentinel-1 and Sentinel-2 indices allowed the dates of the germination, tillering, jointing heading, maturity, and harvesting stages to be determined with the support of the crop calendar. (2) The $TNPI_{increase}$ and $TNPI_{decrease}$ revealed that the declining part of the NDVI profile from $NDVI_{Max}$, to $NDVI_{Min2}$ revealed higher TNPI values (from 0.58 to 1) than the rising part (from 0.08 to 0.58). (3) The most accurate models for predicting phenological stages were generated from the WDVI and VH–VV remote sensing indices, having an R^2 equal to 0.70 from germination to jointing and an R^2 equal to 0.84 from heading to maturity.

Keywords: crop monitoring; Sentinel-1; Sentinel-2; time-series; Google Earth Engine; Temporal Normalized Phenology Index (TNPI)

Citation: Saad El Imanni, H.; El Harti, A.; Panimboza, J. Investigating Sentinel-1 and Sentinel-2 Data Efficiency in Studying the Temporal Behavior of Wheat Phenological Stages Using Google Earth Engine. *Agriculture* **2022**, *12*, 1605. https://doi.org/10.3390/agriculture12101605

Academic Editor: Josef Eitzinger

Received: 22 August 2022
Accepted: 21 September 2022
Published: 3 October 2022

1. Introduction

Crop phenology is the study of the seasonal cycle of vegetation growth and development phases. It contains comprehensive information about developments at the stages of the crop growing season, which is useful for analyzing the impact of climate change on crops in a specific region [1]. From this perspective, the continuous monitoring of the phenological status of crops is required for improving irrigation, fertilization, and pesticide application [2]. The original motivation of this article was the precise and continuous monitoring of phenological stages of wheat on a field and regional level using Sentinel-1, Sentinel-2, and GEE in a semi-arid and fragmented agricultural region, i.e., the case of the

Tadla Irrigated Perimeter (TIP) in central Morocco. The TIP was chosen as a study area due to its agricultural importance in the region, particularly in cereals production [3].

Recent studies in the TIP focused on crop type mapping from Landsat 8 NDVI data [4], crop classification using Sentinel-2 time series [5], the monitoring of surface soil moisture by applying optical data [6], and the monitoring of soil salinization using satellite spectral indices [3]. However, a cloud computing approach based on the evaluation of the remote sensing indices derived from Sentinel-1 and Sentinel-2 in studying the phenological stages of wheat and developing an accurate phenology model is still not developed in the region.

Vegetation phenology using remote sensing is advantageously used for providing spatial and temporal information on crop growth [1]. Optical satellite imagery is one of the most interesting data types used to study the links between the photosynthetic and optical properties of plant leaves based on spectral bands and vegetation indices [7,8]. Synthetic Aperture Radar (SAR) remote sensing is an active remote sensing method that provides cloud-free imagery in all weather conditions, day and night [8,9] Furthermore, SAR sensors are sensitive to the target surface's "roughness" and "wetness", providing additional information on the type of vegetation cover [9].

The recent SAR Sentinel-1 and optical Sentinel-2 sensors, developed by the European Space Agency are freely available and provide crop monitoring at a high spatial and temporal resolution [10]. Sentinel-1A was launched in 2014 and began providing images every 12 days, with this resolution being improved to 6 days by the launch of Sentinel-1B. Sentinel-2A launched in 2015, providing data at a time interval of 10 days, and the launch of Sentinel-2B allowed images to be acquired every 5 days. Additionally, the data have a very high spatial resolution of 10 m, which is suitable for monitoring crops at the plot level [11,12].

Many studies have evaluated the use of multi-temporal Sentinel-1 and Sentinel-2 data in identifying the phenological stages of crops. The most significant aspect of SAR remote sensing to determine temporal changes in crop phenology is the assessment of multi-temporal, multi-polarization, and multi-frequency synthetic aperture radar (SAR) images [11]. In the Bekaa plain of Lebanon, Nasrallah et al. [2] revealed that the Sentinel-1 data were suitable for estimating the dates of phenological stages given the notable variations in the Sentinel-1 time series at the growth stages. The spectral indices calculated with visible and near infrared wavelengths are highly useful for crop discrimination. There are several tools for identifying crop phenology, with the most commonly used method being the Normalized Difference Vegetation Index (NDVI) threshold [12]. However, the Temporal Normalized Phenology Index (TNPI) is predicted to provide a better comprehension of phenological changes at two phases than utilizing single NDVI data [13]. In India, Vaghela et al. [1] used the TNPI derived from Sentinel-2 to produce the crop growth profiles of wheat and mustard crops.

The use of both optical and SAR data is an essential tool for the accurate monitoring of phenological stages [14]. In Northeast Germany, Harfenmeister et al. [15] detected the phenological stages of winter wheat and winter barley using time series of Sentinel-1 and Sentinel-2. Moreover, Mercier et al. [16] found that the use of Sentinel-1 and Sentinel-2 allowed for the identification of the beginning and end of tillering for wheat and the beginning and end of ripening for rapeseed in northern France.

Several methods, including biophysical crop-simulation models, crop growth models, agrometeorological models, and machine learning models [17,18] have been developed to forecast crop phenology parameters using remotely sensed data, where statistical regression methods are the most commonly used approaches [19,20]. Using remote sensing data, more complicated machine learning models have been utilized to anticipate agricultural estimations as yield [21]. Machine learning models have the disadvantage of being less interpretable than regression models with a priori functional form requirements. The regression models are founded on empirical relationships between in-situ parameters, measurements, and vegetation indices [18,22].

Moroccan agriculture monitoring offers a lot of potential for quality improvement. The efficiency of the recent Google Earth Engine (GEE) platform in terms of remote sensing accessibility and reductions in processing time, computation, and automation, could aid in the more effective monitoring of agricultural phenological information at specific stages.

Therefore, this paper was planned as follows: (1) to evaluate the temporal profiles of Sentinel-1 and Sentinel-2 data in extracting the dates of the phenological stages of wheat from germination tomature plant using the GEE JavaScript interface, (2) to assess the relationship between phenological stages and optical/ SAR remote sensing indices in order to develop an accurate phenology estimation model of wheat and extrapolate it to the regional scale.

2. Study Area

The Tadla Irrigated Perimeter (TIP) is located between 32°12′0″ N 7°0′0″ W and 32°24′0″ N 6°24′0″ W in central Morocco and has an average altitude of 400 m (Figure 1). The TIP is one of the most important large-scale irrigation systems in Morocco and covers over 100,000 hectares of irrigated land. It is separated into two compartments: the Beni Amir perimeter on the Northern bank and the Beni Moussa perimeter on the Southern bank. Temperatures range from 6 °C in January to 48 °C in August, and the climate is arid to semi-arid [3]. The average annual rainfall is 280 mm, with significant annual variability. The terrain is mostly fragmented and heterogeneous, with 86% of parcels being less than 5 ha and only 5% percent being larger than 10 ha [4].

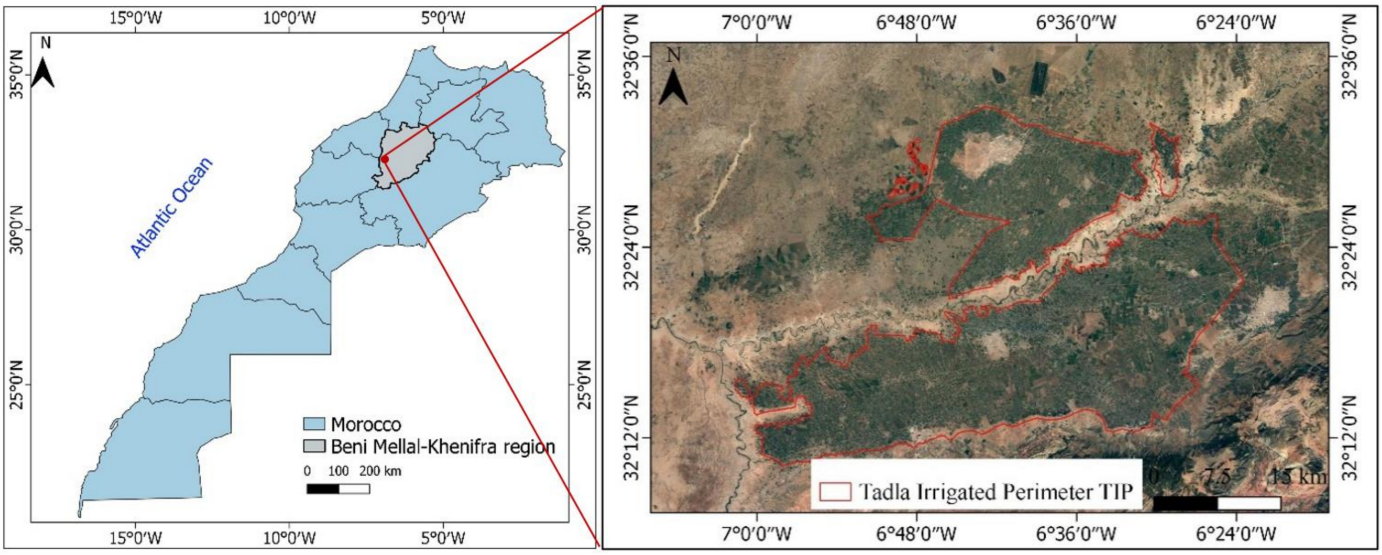

Figure 1. Location of the study area at the national scale (**left**). Scene of Tadla Irrigated Perimeter (**right**).

3. Study Area and Datasets

3.1. Study Area

Field surveys were conducted on nine fields of wheat from November 2020 to May 2021 (Figure 2). The coordinates of the fields were recorded using a GPS. The sizes of the plots ranged from 13 ha and 42 ha (mean = 21.41 ha, median = 17 ha). The height of the measured plants varied from 10 cm and 140 cm throughout the growing season of the wheat plots.

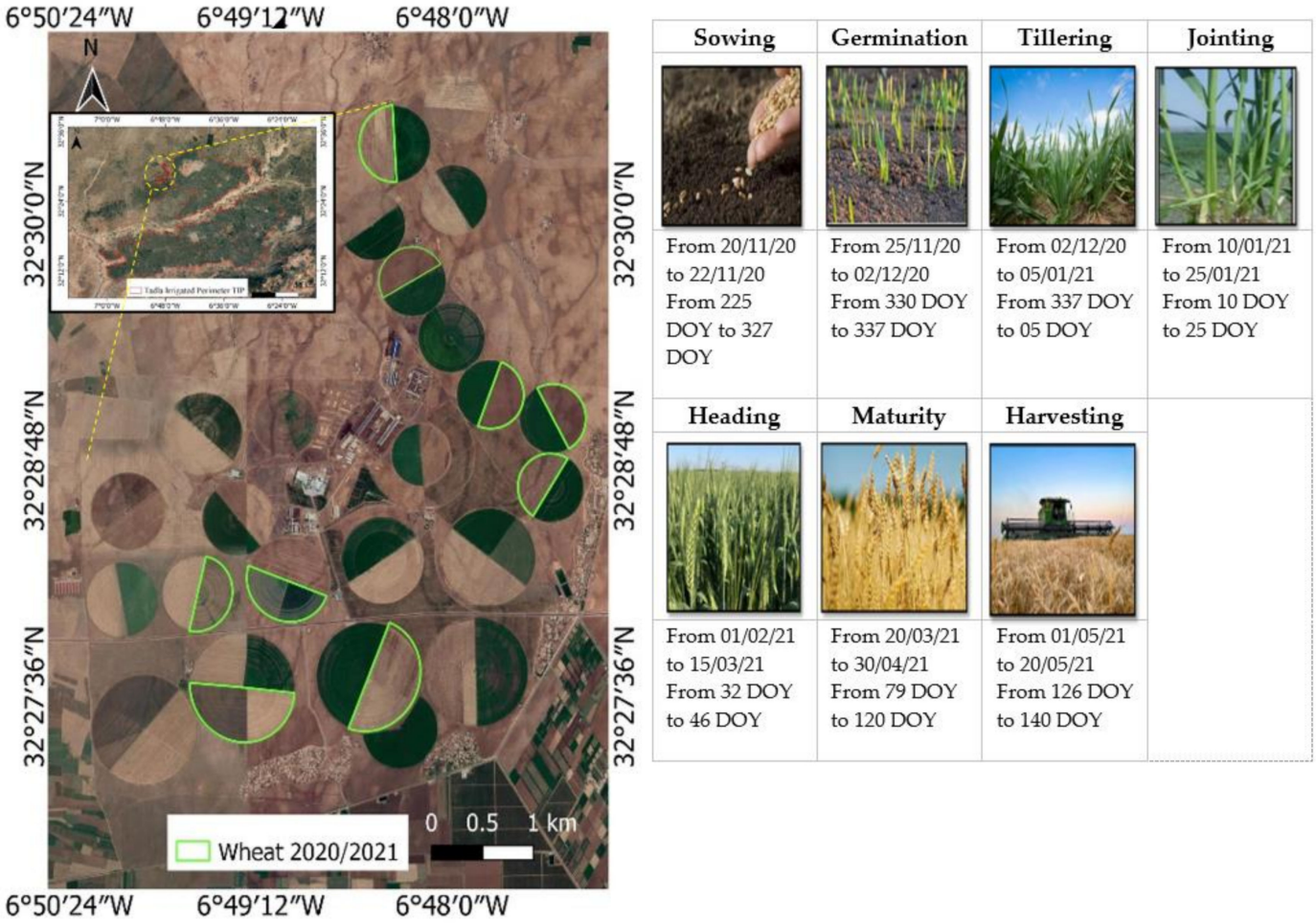

Figure 2. Location of wheat fields for the growing season 2020/2021 (**left**) and calendar of the phenological stages of wheat (**right**).

Seven phenological stages have been observed in the field: sowing, germination, tillering, jointing, heading, maturity, and harvesting (Figure 2). In the germination phase, wheat seeds need appropriate temperatures and humidity to germinate. Seedling emergence normally happens within seven days under ideal conditions. Until the first leaf develops, the seedling will depend on the energy and nutrients contained in the seed. Concerning the application of fertilizer, different studies have demonstrated that nitrogen can be applied after sowing and/or during tillering. As a result, it is critical to remember that once heading is reached (where the head will fully emerge from the stem), any additional nitrogen will result in nitrogen loss and low nitrogen-use efficiency, resulting in a massive decline in overall system efficiency and final net profit in addition to environmental effects [2]. Furthermore, wheat farmers apply fungicides as soon as the flag leaf appears and continues to grow until it has fully expanded in the jointing phase. When the flag leaf has fully developed, the heading phase begins, and any fungicidal application must cease at this point. Following heading, the plant starts flowering. In the maturity stage, the plant dries and becomes extremely rigid. A calendar of sowing, germination, heading, maturity, and harvesting of winter cereals is presented in Figure 2.

3.2. DataSets

3.2.1. Optical Data

The Sentinel-2 Multi-Spectral Instrument (MSI) is positioned aboard two orbiting satellites (Sentinel-2 A/B) which provide a high spatial and temporal resolution (10 m, 20 m, and 60 m every 5 days) [23]. The MSI includes 13 spectral bands (Table 1). This study

used the Level-2A product, which provides Bottom Of Atmosphere (BOA) reflectance images. The criterion for filtering the satellite imagery was that the scenes should contain minimal or no clouds (less than 1% cloud cover). The Sentinel-2 spectral bands were used to create the temporal profiles of spectral bands and to compute the vegetation indices.

Table 1. Characteristics of Sentinel-2 MSI L2A images.

Band	Description	Resolution	Wavelength
B1	Aerosols	60 m	443.9 nm (S2A)/442.3 nm (S2B)
B2	Blue	10 m	496.6 nm (S2A)/492.1 nm (S2B)
B3	Green	10 m	560 nm (S2A)/559 nm (S2B)
B4	Red	10 m	664.5 nm (S2A)/665 nm (S2B)
B5	Red Edge 1	20 m	703.9 nm (S2A)/703.8 nm (S2B)
B6	Red Edge 2	20 m	740.2 nm (S2A)/739.1 nm (S2B)
B7	Red Edge 3	20 m	782.5 nm (S2A)/779.7 nm (S2B)
B8	NIR	10 m	835.1 nm (S2A)/833 nm (S2B)
B8A	Red Edge 4	20 m	864.8 nm (S2A)/864 nm (S2B)
B9	Water vapor	60 m	945 nm (S2A)/943.2 nm (S2B)
B11	SWIR 1	20 m	1613.7 nm (S2A)/1610.4 nm (S2B)
B12	SWIR 2	20 m	2202.4 nm (S2A)/2185.7 nm (S2B)

3.2.2. SAR Data

Sentinel-1 is a constellation of two polar-orbiting satellites (Sentinel-1 A/B) that operate day and night providing images every 6 days. The Sentinel-1 observation system uses the wide interferometric mode (IW) as the predefined mode on land. This mode produces dual-polarized, i.e., vertical transmit/receive (VV) and vertical transmit/horizontal receive (VH), images, with a spatial resolution of 10 m [24,25] (Table 2). In this study, the Level-1 Ground Range Detected (GRD) was acquired in the descending orbit products. The preprocessing of SAR imagery consists of (1) applying the orbit file; (2) GRD border noise removal; (3) thermal noise removal; (4) radiometric calibration; (5) terrain correction (orthorectification); and (6) conversion to a backscattering coefficient (σ0) in decibels (dB), provided by GEE [26].

Table 2. Characteristics of Sentinel-1 images.

Band	Polarization	Mode	Wavelength	Pixel Size	Product Level	Product Type
C band	Vertical transmit and vertical receive (VV)	Interferometric Wide (IW)	5.6 cm	10 m	Level-1	Ground Range Detected
	Vertical transmit and horizontal receive (VH)		5.6 cm	10 m		

A series of 20 Sentinel-2 and 36 Sentinel-1 images covering the period from November 2020 to May 2021 were employed in this study (Table 3).

3.2.3. Meteorological Data

Rainfall and temperature affect plant growth and the rate of phenological stages [27]. For this study, the rainfall and temperature data were recorded almost every 10 days from September 2020 to July 2021 in the TIP (Figure 3).

Table 3. Sentinel-1 and Sentinel-2 acquisition dates.

Month	Dates of Acquisition Sentinel-2 (MSI)	Days of Year (DOY)	Dates of Acquisition Sentinel-1 (SAR)	Days of Year (DOY)
November 2020	2, 17, 22	307, 322, 327	1, 7,13, 19, 25	306, 311, 318, 324, 330
December 2020	2, 12, 22, 27	337, 347, 357, 362	1, 7, 13, 19, 25,31	336, 342, 348, 354, 360, 366
January 2021	01, 16, 26, 31	01, 16, 26, 31	6, 12, 18, 24, 30	6, 12, 18, 24, 30
February 2021	10, 15	41, 46	5, 11, 17, 23	36, 42, 48, 54
March 2021	12, 22	71, 81	1, 7, 13, 19, 25, 31	60, 66, 72, 78, 84, 90
April 2021	01	91	6, 12, 18, 24, 30	96, 102, 108, 114, 120
May 2021	6, 11, 16, 22	126, 131, 136, 141	6, 12, 18, 24, 30	126, 132, 138, 144, 150

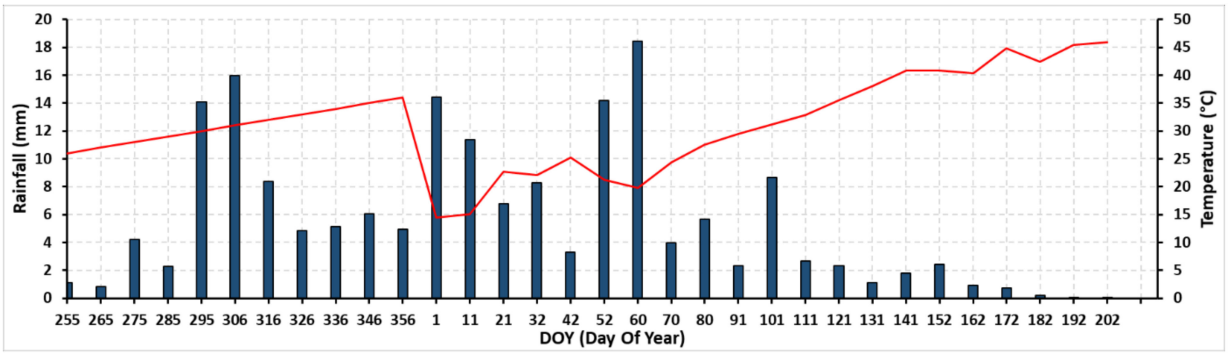

Figure 3. An ombrothermal diagram of climatic conditions in the TIP from September 2020 to July 2021 (precipitation is represented by the blue bars and temperature by the red line).

4. Methods

The methodological approach was developed to precisely monitor the wheat plots and to develop a forecast phenological model based on remote sensing parameters derived from Sentinel-1 and Sentinel-2 time series. The methodology is divided into four sections. Firstly, the temporal profiles derived from Sentinel-1 and Sentinel-2 remote sensing data were evaluated in terms of extracting the dates of the phenological stages in agreement with the phenological calendar of the wheat observed in-situ. Secondly, the remote sensing indices were used for assessing the relationships between phenological stages as input for the estimation model of phenological stages. The dates of the phenological stages recorded were the independent variables of the regressions. The dependent variables included the remote sensing indices. Thirdly, the greatest optical and radar remote sensing indices in terms of the prediction of phenological stages were deduced and chosen as input for the estimation of phenological seasons. Fourthly, the phenological models were developed and the mapping of the wheat of the TIP for the season 2020/2021 was obtained in order to extrapolate the phenological estimation for the wheat fields of the season 2020/2021 at the TIP regional scale. The methodological approach was developed and analyzed with the GEE cloud computing platform and MATLAB software (Figure 4).

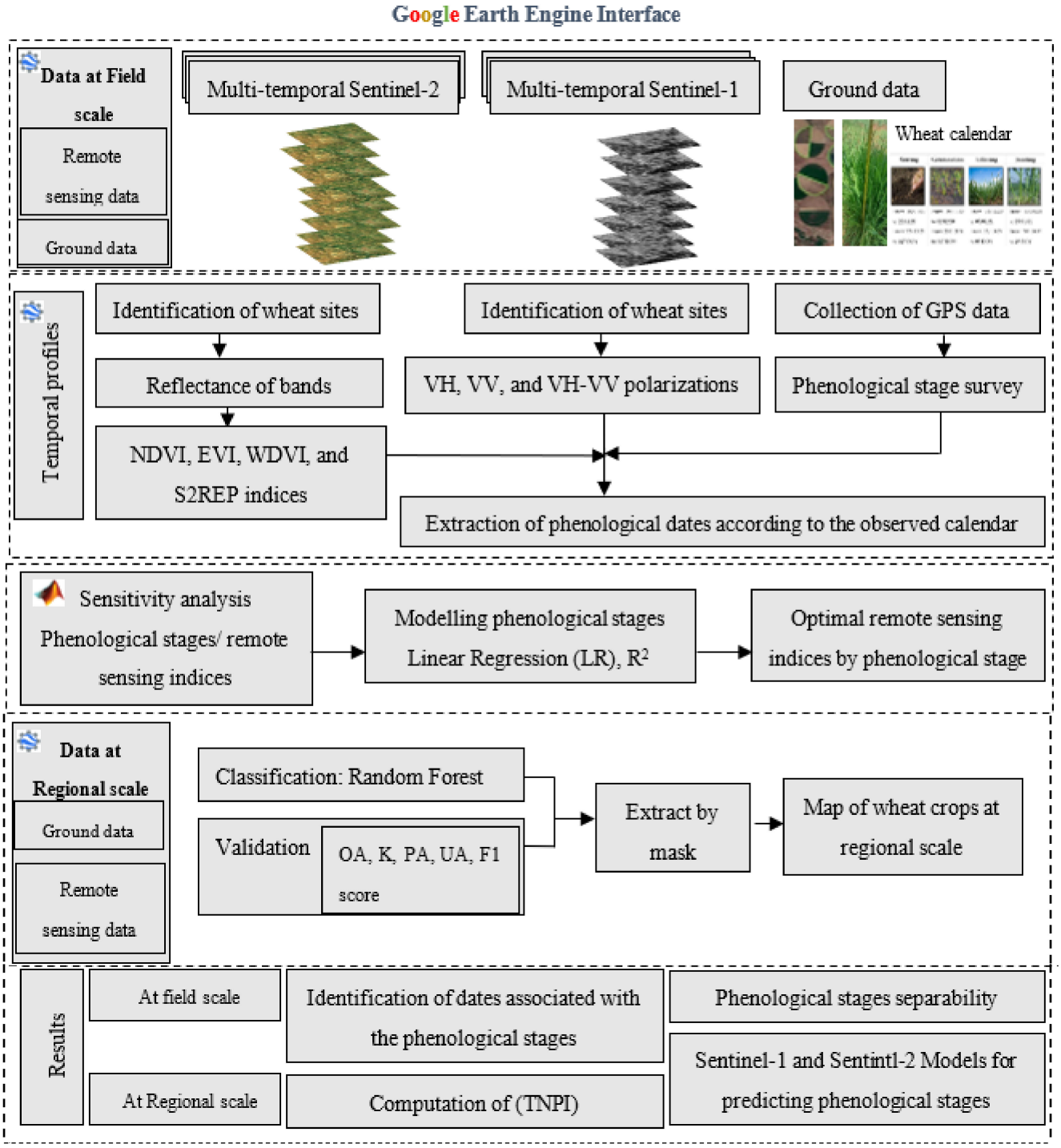

Figure 4. Flowchart of the proposed method to predict the phenological stages of wheat using the Google Earth Engine.

4.1. Temporal Profiles of Spectral Bands

Time series remote sensing data are a useful source for monitoring and predicting the phenological and ecological characteristics of vegetation [24]. Sentinel-2 imagery, with its thirteen spectral bands, is effective in describing the spectral responses of vegetation [25]. In this first step, the temporal profiles of spectral bands were established and analyzed from the multi-temporal Sentinel-2 images for the following bands: B2, B3, B4, B6, B7, B8, B8A, B11, and B12. An average profile of each spectral band derived from the sampled wheat was examined.

4.2. Temporal Profiles of Vegetation Indices

The temporal profiles of the Normalized Difference Vegetation Index (NDVI), the Enhanced Vegetation Index (EVI), the Weighted Difference Vegetation Index (WDVI), and the Sentinel-2 Red Edge Position (S2REP) were plotted based on the mean values derived from the sampled wheat.

The Normalized Difference Vegetation Index (NDVI) is one of the most important vegetation indices [1,26,27]. The NDVI time series curve is a practical method for identifying the phenological stages and growing conditions of crops, such as germination, tillering, jointing, heading, maturity, and harvesting. NDVI is derived from reflectances in the red (R) and near-infrared (NIR) portions of the spectrum [28] (Table 4).

The Enhanced Vegetation Index (EVI) has attracted considerable attention in the context of monitoring the quality and quantity of vegetation. It is represented as an optimized vegetation index to provide an improved vegetation signal with higher sensitivity in areas with dense biomass [29]. The EVI is calculated from reflectances in the red (R), blue (B), and near-infrared (NIR) portions of the spectrum [28] (Table 4).

The Weighted Difference Vegetation Index (WDVI) is distinct from ratio indices, as it is a distance-based index that was developed for correcting the near-infrared reflectance of soil background [30–32] (Table 4).

The Sentinel-2 Red Edge Position (S2REP) developed especially for Sentinel-2 [33] demonstrates the difference between maximum absorption in the red part and reflectance in the NIR portion [34]. The S2REP red-edge index is based on a linear interpolation approach based on the work of Guyot and Baret [35] by using Sentinel-2 bands 8 and 4 [36] (Table 4).

Table 4. Vegetation indices calculated from Sentinel-2 images. R = Red, RE = Red-Edge, NIR = Near-infrared, NDVI = Normalized Vegetation Index, EVI = Enhanced Vegetation Index, WDVI = Weighted Difference Vegetation Index, S2REP = S-2 Red-Edge Position index.

Index	Equation	S-2 Bands Used	Original Author
NDVI	(NIR − R)/(NIR + R)	(B8 − B4)/(B8 + B4)	[37]
EVI	2.5(NIR − R)/(NIR + 6R − 7.5BLUE + 1)	2.5(B8 − B4)/(B8 + 6B4 − 7.5B2 + 1)	[38]
WDVI	(NIR − 0.5 × R)	(B8–0.5 × B4)	[30]
S2REP	705 + 35 × (((NIR + R)/2)-RE1)/(RE2 − RE1))	705 + 35 × (((B7 + B4)/2) − B5)/(B6 − B5))	[35]

4.3. Temporal Profiles of Backscattering Coefficients

The use of the backscattering coefficient, provided by the Sentinel-1, yielded additional information for monitoring crop phenology [16]. In this context, two modes of polarization were processed: vertical transmit/receive (VV) and vertical transmit/horizontal receive (VH), which have been used for computing the backscatter (σ○) of the difference (VH–VV) polarization.

4.4. Phenological Sages Separability Using Optical and SAR Parameters

To investigate the separability of the phenological stages, the scatterplot of the field samples including the vegetation indices and the VH, VV, and VH–VV polarization was analyzed. For this purpose, the combinations of (NDVI, EVI), (NDVI, WDVI), (NDVI, S2REP), (VH, VV), (VH, VH–VV), and (VV, VH–VV) were selected.

4.5. Sensitive Analysis between Remote Sensing Indice and Phenological Stages

In this research, a sensitive analysis between Sentinel-1 and Sentinel-2 indices and the dates of phenological stages was evaluated by the coefficient of determination (R2), the Root Mean Square Error (RMSE), and the normalized nRMSE. The R2 measures the

prediction quality of the regression model. The RMSE error represents the mean difference between the 'estimated' and 'measured' dates of phenological stages.

$$R^2 = 1 - \frac{\sum_{i=1}^{n}(P_i - M_i)}{\sum_{i=1}^{n}(\overline{M} - M_i)} \quad (1)$$

$$RMSE = \sqrt{\sum_{i=1}^{n}(P_i - M_i)^2 / n} \quad (2)$$

$$nRMSE = \frac{RMSE}{\overline{M}} \times 100 \quad (3)$$

* where n, P_i, M_i, and $\overline{M}$ represent numbers of samples, predicted values, measured values, and the mean value of M_i, respectively.

4.6. Crop Classification

To upscale the monitoring of phenological stages from the nine wheat fields to the entire study area, a crop classification map for the TIP was performed. This map was generated by employing the pixel-based image classification of the multi-temporal Sentinel-1 and Sentinel-2 data and RF classifier. The Random Forest (RF) algorithm developed by Breiman et al. [39] can be defined as an ensemble of several decision trees, with each tree contributing a single vote for the most frequent class [40]. The RF classifier is more competent, and it avoids the overfitting problem associated with, Decision Tree (DT) classifiers by building a set of DTs [39]. Practically speaking, RF develops several DT classifiers for the training and outputting of classes for each tree. [41]. Several studies on crop classification have proved the performance of RF in crop identification [26].

The traditional bands (Blue, Green, and Near Infrared), SWIR bands, red-edge bands, vegetation indices (NDVI and EVI), and the backscattering at co-polarization VV (vertical–vertical) and at cross-polarization VH (vertical–horizontal) were used as inputs. The training data included 736 plots, where 512 were for training (70%) and 224 were for validation (30%). The overall accuracy (OA), Kappa coefficient, user's accuracy, producer's accuracy, and F1 score were used to validate the accuracy of the classification. To generate the wheat land cover over the study area, the wheat class from the crop classification result was extracted and converted to vector format.

4.7. Validation of the Crop Classification

The accuracy of the crop classification result was assessed using five confusion metrics, including overall accuracy (OA), Kappa coefficient, user accuracy (UA), producer accuracy (PA), and F1 score. For each class, 70% of the ROIs were randomly selected for training, and the remaining 30% of ground survey points were used to analyze the accuracy. The OA was calculated by summing the number of correctly classified cells and dividing this by the total number of cells, while the Kappa coefficient measures the proportion of errors that are minimized by classification and completely random classification.

The PA is the conditional probability that the classification output of a particular location on the classification map is compatible with any random sample in the test data.In contrast, the UA consists of selecting a random sample with the same conditional probability as the actual type of ground from the classification results [42]. PA and UA were computed from the error matrix of classification.

The F1 score is an important metric that balances the difference between PA and UA for each class by the formulation of the harmonic mean of PA and UA [43]. These accuracies were calculated as presented in the equations below.

$$OA(\%) = \frac{\sum_{i=1}^{n} p_{ii}}{N} \times 100 \quad (4)$$

$$Kappa = \frac{N\sum_{i=1}^{n} p_{ii} - \sum_{i=1}^{n}(p_{i+} \times p_{+i})}{N^2 - \sum_{i=1}^{n}(p_{i+} \times p_{+i})} \quad (5)$$

$$UA(\%) = \frac{p_{ii}}{p_{i+}} \times 100 \quad (6)$$

$$PA(\%) = \frac{p_{ii}}{p_{+i}} \times 100 \quad (7)$$

$$F1\ score(\%) = \frac{UA \times PA}{UA + PA} \times 2 \quad (8)$$

* where n is the total number of columns of the confusion matrix; p_{ii} is the number of correct classifications of the upper crop-type sample in the i row and i column of the confusion matrix, p_{i+} and p_{+i} are the total number of crop-type samples in row i and column i, and N is the total number of samples used for verification.

4.8. Computation of TNPI and Temporal Change Analysis

The TNPI is a temporal index that quantifies the change between two periods. When employed to the start and the peak of the vegetative cycle, it evaluates the growth between these two times. Unlike other phenological indices, the TNPI only requires two time steps rather than the complete temporal sequence of the vegetation period, resulting in a reduction in the amount of time-series data to be analyzed. The proposed temporal index is predicted to improve knowledge of phenological changes at two phases when compared with utilizing single NDVI data [13]. The TNPI can be computed as follows:

$$TNPI = \frac{NDVI_{Max} - NDVI_{Min}}{NDVI_{Max} + NDVI_{Min}} \quad (9)$$

* where $NDVI_{Min}$ is the minimum and $NDVI_{Max}$ is the maximum NDVI value of the vegetative cycle.

For this purpose, the NDVI growth profile for the entire wheat crop season was used to create a composite image from three dates, including the minimum value NDVI during the beginning growth phase, the maximum value NDVI during the peak growth stage, and the minimum value NDVI before the harvesting phase. Temporal Normalized Phenology Index (TNPI) images were computed to monitor TNPI-based crop growth changes in the TIP agricultural region, reflecting an increase in TNPI and a decrease in TNPI. The values generated were scaled between 0 and 1. This scale indicates the temporal change in vegetation greenness throughout wheat areas, with 0 representing no temporal change and 1 being the largest temporal change.

5. Results

5.1. Sentinel-2 Temporal Profiles

5.1.1. Temporal Profiles of Sentinel-2 Spectral Bands

The mean values in each spectral band for wheat crops were computed for various dates to identify specific growth stages where the temporal behavior of the spectral bands differs between phenological stages. Predominantly, the spectral–temporal profile of wheat crops (Figure 5) matches the typical spectral profile of the photosynthetic vegetation, showing decreasing values in the Red (B4) and SWIR (B11, B12) bands and increasing values in the NIR (B8, B8A) bands and red-edge bands (B6, B7) over time (based on the vegetation development). The highest signal variations were observed for the red-edge and NIR bands, while the lowest signal variations were noted for the RGB bands. From Figure 5, it can be considered that the growth period begins from the 337 DOY, when the reflectance values of NIR and red-edge bands start to increase, symbolizing the germination stage. The highest vegetation development was rerecorded between 41 DOY and 81 DOY, corresponding to

the heading stage, a phase in the growth of plants marked by the emergence of a head from the sheath of the upper leaf.

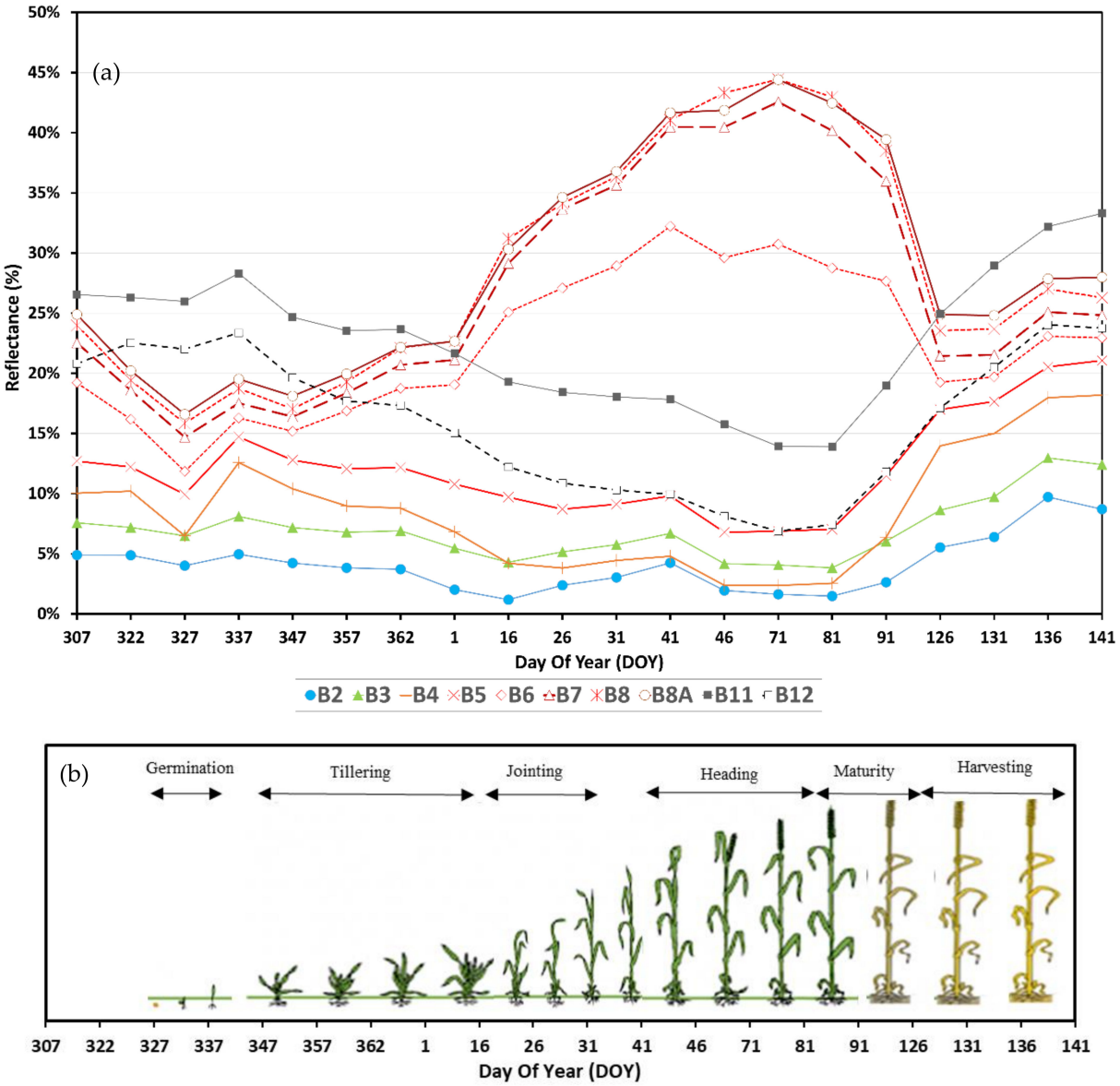

Figure 5. Mean temporal profiles of Sentinel-2 reflectance (**a**) and main phenological stages for wheat (**b**).

5.1.2. Temporal Profiles of Vegetation Indices

The mean temporal profiles of Sentinel-2 vegetation indices for wheat plots were generated during the growing season (Figure 6). The profiles include on each date, the average vegetation index of the reference plots. The NDVI, EVI, WDVI, and S2REP values began to increase at the beginning of germination until the heading stage, while they all decreased during maturity and harvesting. NDVI showed maximum values compared to EVI and WDVI.

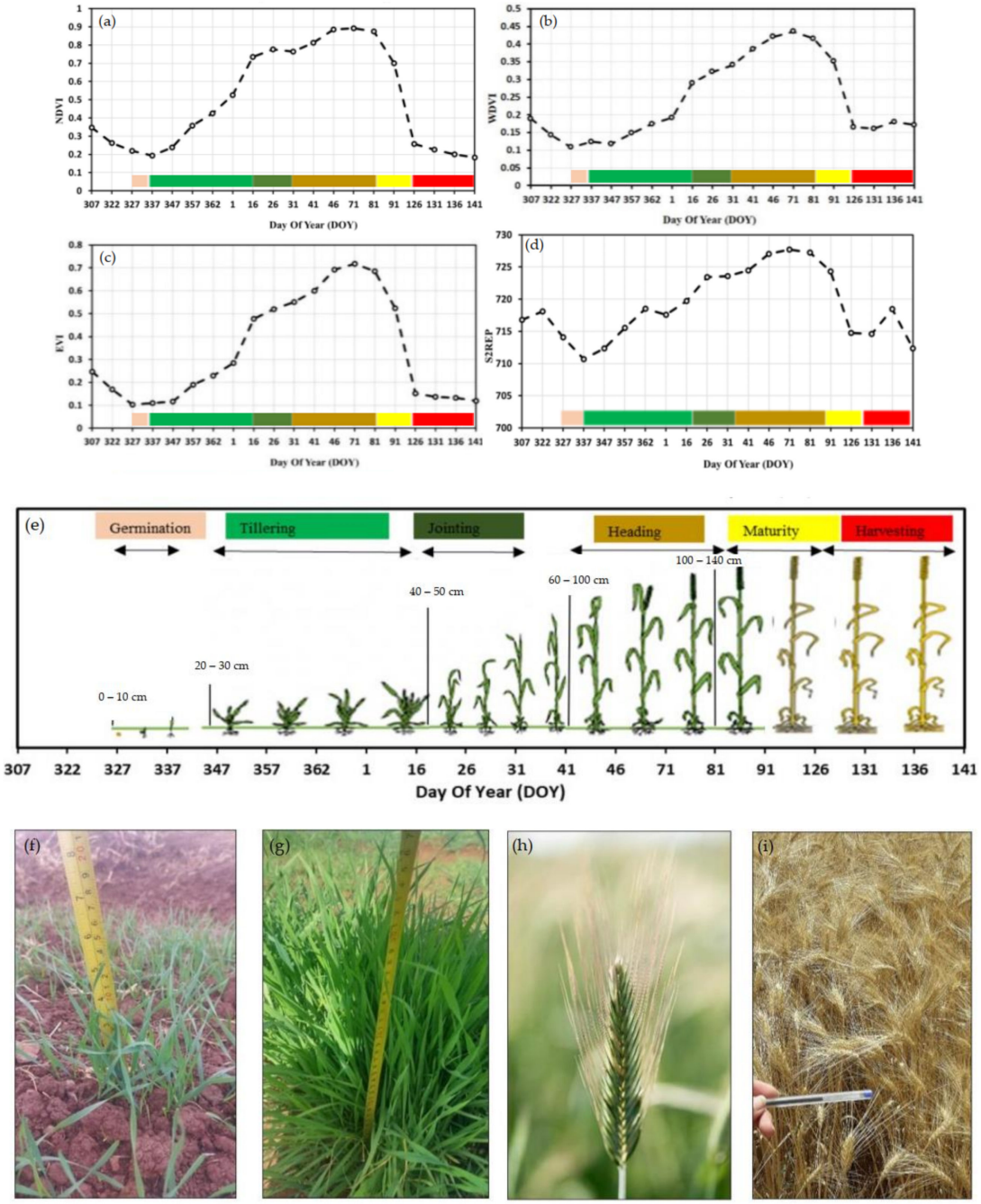

Figure 6. Mean temporal profiles of Sentinel-2 vegetation indices (**a**–**d**) main crop phenological stages survey for wheat plots and measured height of wheat plant (**e**–**i**). NDVI = Normalized Vegetation Index, EVI = Enhanced Vegetation Index, WDVI = Weighted Difference Vegetation Index, S2REP = S-2 Red-Edge Position index.

Sowing had taken place in late November, after rain events, ensuring sufficient soil moisture for germination. The germination period was recorded between 327 DOY and 337 DOY, which corresponds to the phenological phase when the plant first arises from a seed. During the germination process, the plant does not grow taller than 10 cm. From this stage, the vegetation indices values continue to increase, ensuring the development of the plant.

Constant vegetation indices values were observed from 26 DOY to 31 DOY. This corresponds to the winter dormancy phase, which is marked by a temporary slowing of the growth cycle. Following this period, the vegetation indices values rise once more until reaching a maximum peak recorded on 71 DOY, ensuring the heading of the plant, a phase in the growth of plants characterized by the emergence of a head from the sheath of the upper leaf. The height measured in the field at heading for the wheat plants was from 60 cm to 100 cm. The increased plant biomass, leaf chlorophyll concentration, and nitrogen content during the heading stage are reflected in the higher NDVI, EVI, WDVI, and S2REP values.

At the maturity phase, the plat dries and presents a straw color with a rigid kernel. This stage lasts from 81 DOY to 126 DOY. Consequently, the decline in vegetation indices values at the end of the season was related to physiological maturity, crop color change, and leaf senescence. Harvesting can be carried out after the 126 DOY, when the crop is physiologically mature.

5.2. Temporal Profiles of SAR Backscattering in VH, VV, and VH–VV Polarizations

In this section, the Sentinel-1 polarizations (VV, VH, VH–VV) were evaluated in terms of the detection of each phenological phase (Figure 7). The profiles include, on each date, the average SAR backscatter (σ○) in VH, VV, and VH–VV polarizations of the reference plots. The VH–VV backscatter looks to be more stable over time than VH or VV. Although the VH and VV profiles appear to be complicated, the majority of their variations can be explained physically [14]. During the winter, the vegetation is short and sparse, and VV and VH are primarily influenced by changes in soil backscatter caused by surface roughness. Rainfall events in the germination, tillering, and jointing period may explain the slight increase in the backscatter. Then, until the beginning of the maturity stage, a slight decrease in VV and VH backscatters is recorded, which can be explained by the soil backscatter attenuated by the increase of vegetation.

The SAR backscatter (σ○) in VH–VV polarizations began to increase at the beginning of germination until the heading stage, while it decreased during the maturity and harvesting periods. The period between November and December saw heavy rainfall, reaching 16 mm on 306 DOY, which favored the germination of the wheat plant. Following the optical parameters, the periods of germination, tillering, jointing, heading, maturity, and harvesting was recorded using the VH–VV polarization difference, with an increase in backscatter values with the growth phase of the plant (from germination to heading) followed by a decrease in values after heading. The results show that the backscatter signals of the VH, VV, and VH–VV polarization over wheat crops ranged from −14.52 to −23.92, from −9.25 to −16.27, and from −8.50 to −5.27, respectively, during the complete life cycle of wheat crops.

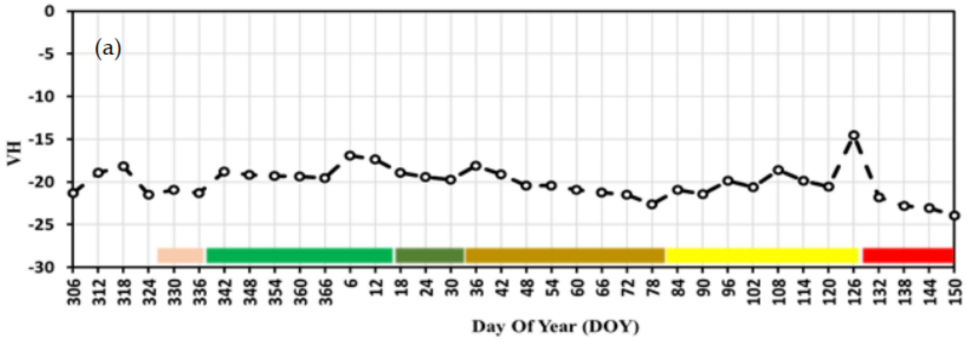

Figure 7. *Cont.*

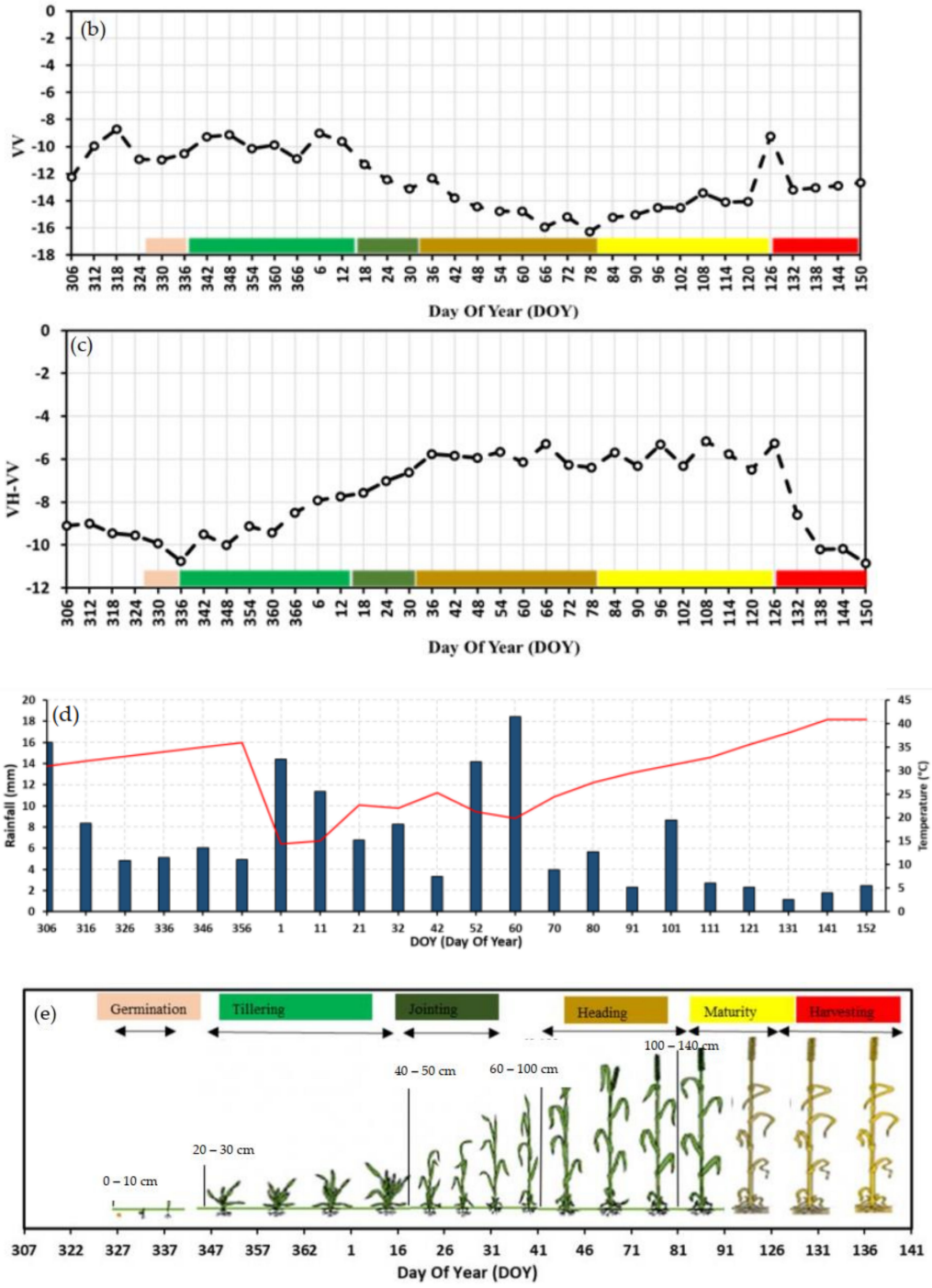

Figure 7. Mean of the Sentinel-1 backscattering coefficients at VH (**a**), VV (**b**), VH–VV (**c**) polarizations, (**d**) the ombrothermal diagram of climatic conditions in the TIP, (**e**) main crop phenological stages survey for wheat plots and measured height of wheat plant.

5.3. Scatter Plot of the Field Samples Comprising Optical and SAR Parameters for the Different Phenological Stages

From the phenological dates, a scatterplot of the nine field samples was created in a space including the NDVI and EVI, NDVI and WDVI, NDVI and S2REP, VV and VH, VV and VH–VV, VH and VH–VV values (Figures 8 and 9).

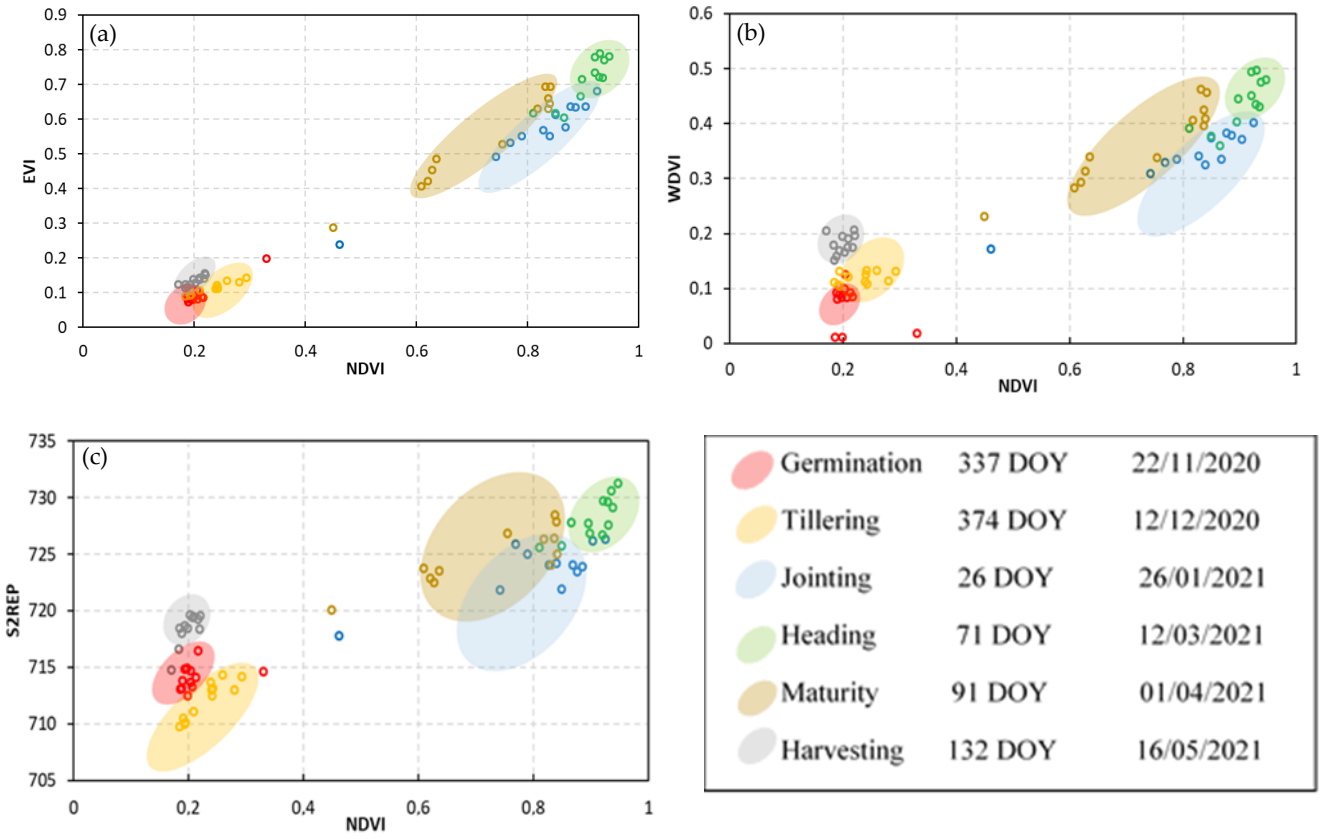

Figure 8. The scatterplot of the field samples of the wheat plots in a space including the NDVI and EVI (**a**), NDVI and WDVI (**b**), NDVI and S2REP (**c**) for the different dates of wheat stages.

The germination stage was more accurately identified using the NDVI and S2REP combination, as the wheat plots showed low NDVI and S2REP values (<0.2 and <715). In the tillering period, the NDVI and S2REP values were discriminated, with the wheat plots showing greater NDVI values (from 0.2 to 0.3) and lower S2REP values (from 710 to 715) than during germination. Using the NDVI and WDVI space combination, the jointing phase was accurately identified. The NDVI and S2REP values for the heading period were distinct, with wheat plots having higher NDVI and S2REP values (>0.8 and >725). The maturity period was discriminated with the NDVI and WDVI space combination. When the crop is mature physiologically, the NDVI and WDVI as well as the NDVI and S2REP space combination, assisted to distinguish the harvesting phase.

However, compared to optical parameters, the combination of VH, VV, and VH–VV polarization was not very effective at differentiating the phenological stages of wheat crops. The germination stage was better identified using the VV and VH–VV space combination, in that VV and VH–VV exhibited lower values (<−10 and <−10). In comparison to other combinations, VV and VH values were more easily distinguished during the tillering period. The jointing phase was more easily distinguished using the VV and VH–VV space combination. The VV and VH–VV values for the heading period were also distinct, with the wheat plots having higher VH–VV and lower VV values (>−8 and <−15). The maturity period was discriminated with the VV and VH space combination. When the crop reached physiological maturity, the VH and VH–VV space combination contributed to distinguishing the harvesting phase.

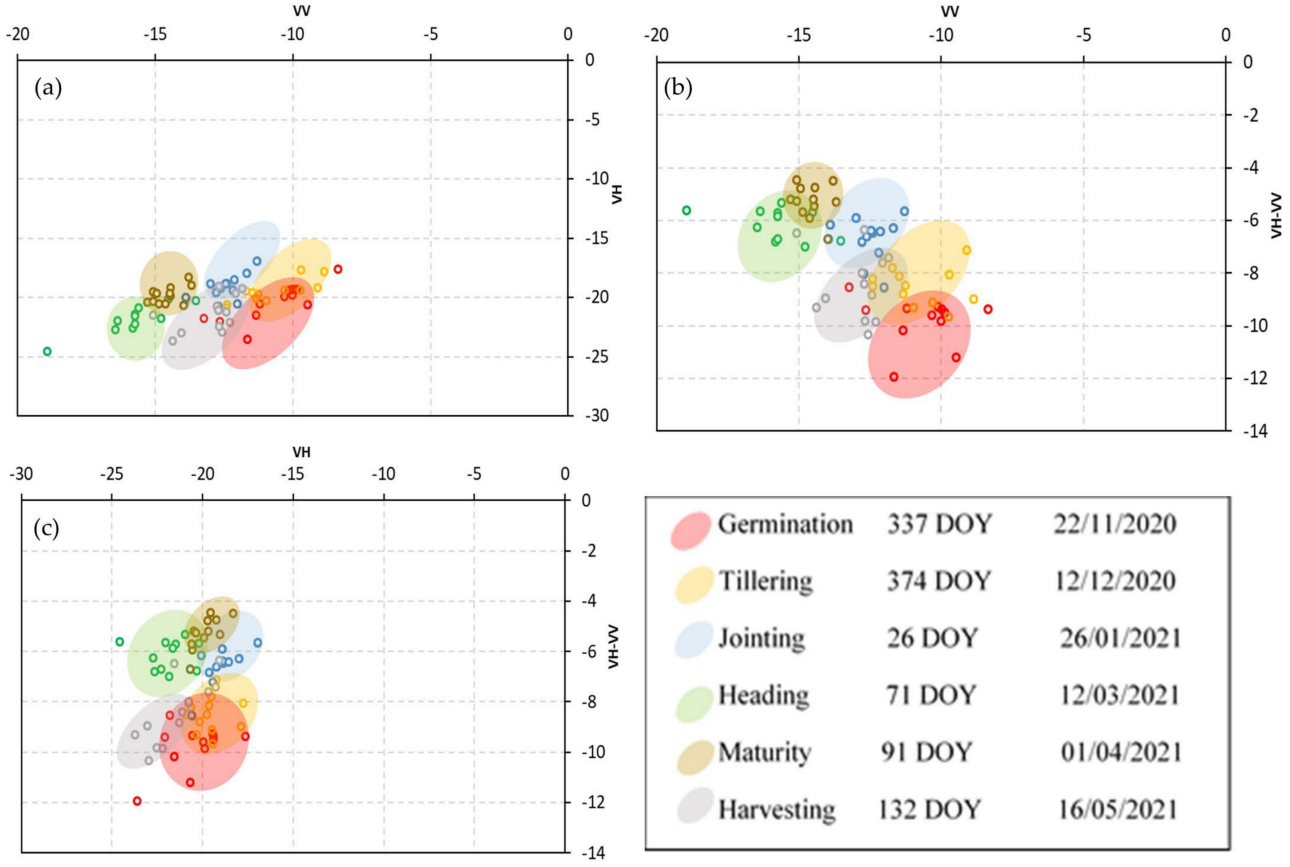

Figure 9. The scatterplot of the field samples of the wheat plots under consideration in a space including the VV and VH (**a**), VV and VH–VV (**b**), VH and VH–VV (**c**) for the different dates of wheat stages.

5.4. Phenology Estimation Model

In this section, four vegetation indices (NDVI, EVI, WDVI, and S2REP) and the tree mode of polarization (VV, VH, and VH–VV) were examined to develop an accurate phenology estimation model. The LR was used as technique to deduce the optimal models, where the vegetation indices and the backscatter were the independent variables and the phonological stages were the dependent variable. The phenological stages are represented as ordinal variables from 1 to 5 (1: germination (337 DOY), 2: tillering (347 DOY), 3: jointing (26 DOY), 4: heading (71 DOY), 5: maturity (91 DOY)). The individual Sentinel remote sensing indices from germination to maturity were evaluated to develop the phanology estimation model equations (Figure 10). The results show that the models had R^2 values ranging from 0.03 to 0.84, an RMSE between 1.39 to 0.56, and an nRMSE from 46% to 18% (Table 5). The model with a higher R^2 value and lower RMSE value represents the most suitable model for phenological stage estimation. The best model based on Sentinel-2 vegetation indices was obtained when using WDVI, with an R^2 = 0.70, RMSE = 0.77, and nRMSE = 26%, while the most suitable model based on Sentinel-1 polarizations was generated when using the VH–VV difference, with an R^2 = 0.84, RMSE = 0.56, and nRMSE = 18%.

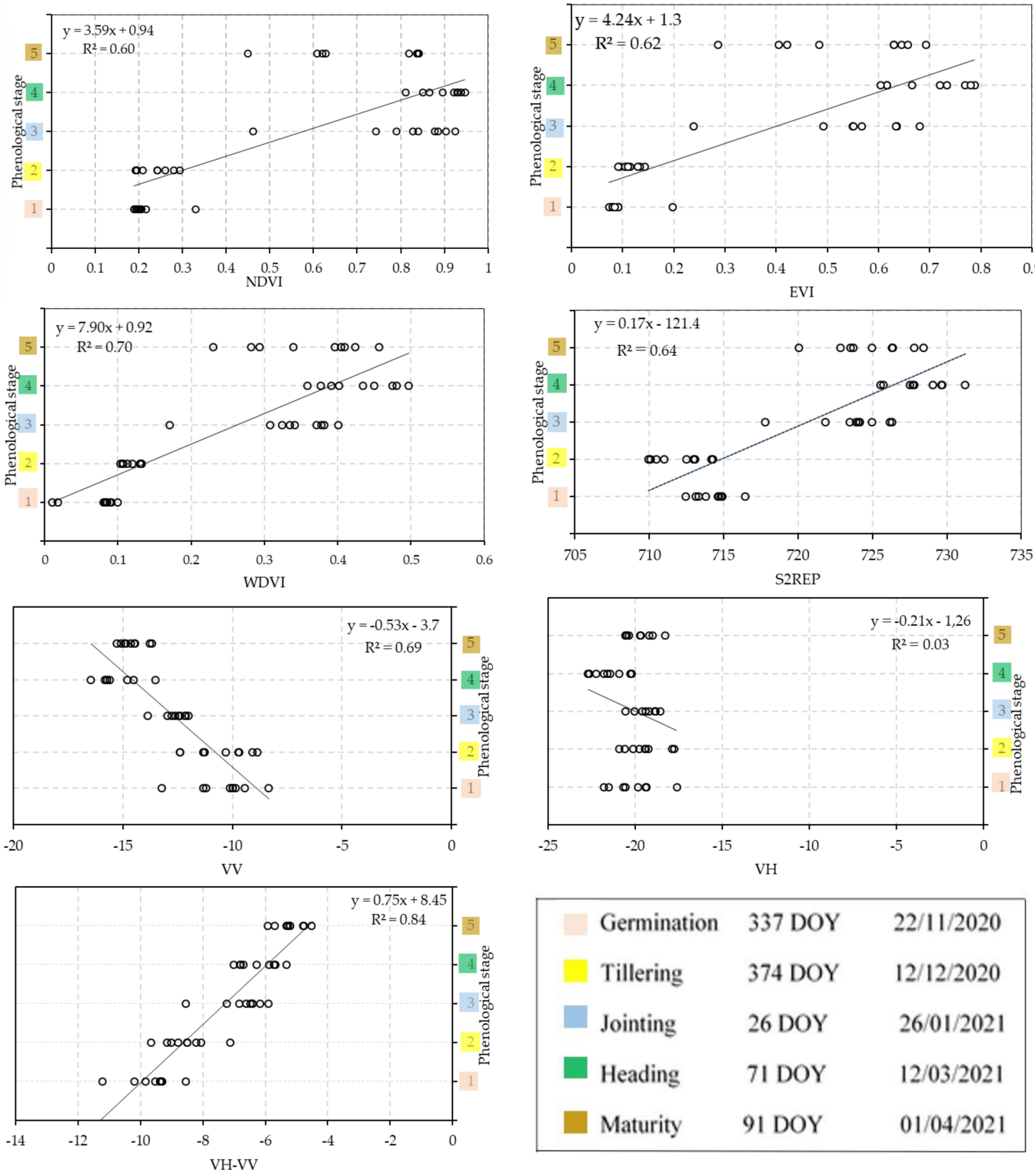

Figure 10. The correlations between phenological stages and optical / SAR remote sensing indices.

Table 5. Phenological models for wheat using optical / SAR remote sensing indices.

MLR Models	Equations	R^2	RMSE	nRMSE (%)
Model 1	$y = 3.59 \times NDVI + 0.94$	0.6	0.89	30%
Model 2	$y = 4.24 \times EVI + 1.30$	0.62	0.87	29%
Model 3	$y = 7.9 \times WDVI + 0.92$	0.7	0.77	26%
Model 4	$y = 0.17 \times S2REP - 121.4$	0.64	2.07	69%
Model 5	$y = -0.53 \times VV - 3.7$	0.69	0.86	29%
Model 6	$y = -0.21 \times VH - 1.26$	0.03	1.39	46%
Model 7	$y = 0.75 \times (VH - VV) + 8.45$	0.84	0.56	18%

5.5. Upscaling the Monitoring of Phenological Stages from the Field to the Regional Scale

The monitoring of wheat phenological stages was upscaled to the entire study area using the wheat crop classification map derived from the RF classification. This map was created by employing the pixel-based image classification of multi-temporal Sentinel-1 and Sentinel-2 data in the early season (from September 2020 to March 2021). The overall accuracy as well as the wheat accuracy parameters, are presented in Table 6.

Table 6. Overall accuracy; Kappa index; wheat user and producer accuracy, and F1 score of the classification result.

Accuracy Index	Accuracy Values
Overall accuracy	95.02%
Kappa index	0.93
Wheat user accuracy	94.61%
Wheat producer accuracy	93.83%
Wheat F1 score	94.22%

5.6. Computation of Temporal Normalized Phenology Index (TNPI)

The NDVI profile was examined to deduce the $NDVI_{Min1}$, $NDVI_{Max}$, and $NDVI_{Min2}$ (Figure 11). The temporal changes in the NDVI were examined by determining the TNPI between different growth phases using Equation (1) in Section 4.5. The TNPI increase (Equation (10)) and TNPI decrease (Equation (11)) were calculated to detect changes in phenological phases from minimum to maximum NDVI values during the wheat growing season. The $NDVI_{Min1}$ at germination (337 DOY), the $NDVI_{Max}$ at heading (71 DOY), and the $NDVI_{Min2}$ prior to harvesting (DOY 126) were computed for the TIP study area (Figure 11).

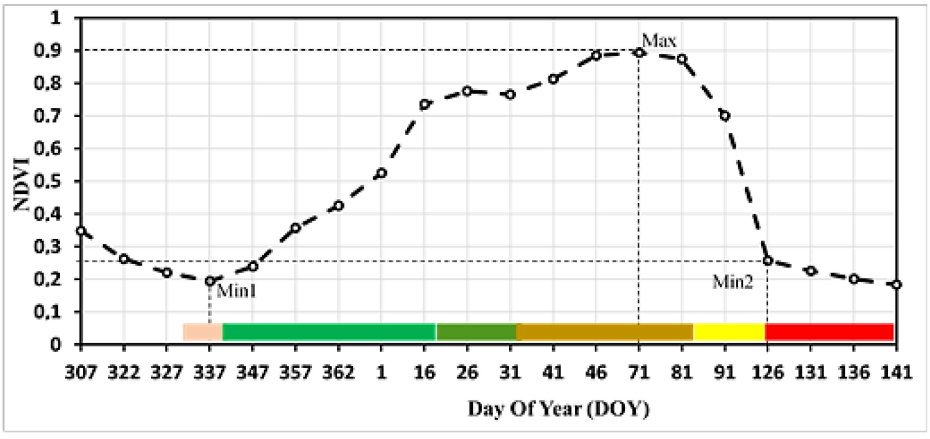

Figure 11. NDVI growth profile of wheat. Min 1: first minimum NDVI, Min2: second minimum NDVI, and Max: maximum NDVI.

$$TNPI_{increase} = \frac{NDVI_{Max} - NDVI_{Min1}}{NDVI_{Max} + NDVI_{Min1}} \quad (10)$$

$$TNPI_{decrease} = \frac{NDVI_{Max} - NDVI_{Min2}}{NDVI_{Max} + NDVI_{Min2}} \quad (11)$$

The increase in TNPI from the germination phase (337 DOY), at Min1 NDVI values, to the heading phase (71 DOY), at Max NDVI values, was computed for the entire study area (Figure 12). Similarly, the decrease in TNPI from heading (71 DOY) to prior to harvesting (DOY 126), at Min2 NDVI values, as shown in Figure 13, was also generated using Equation (3) to monitor changes in crop growth.

The TNPI increase quantifies the change between the germination and heading period. The TNPI increase values obtained are evenly distributed throughout the study area, ranging from 0.08 to 0.58 (Figure 12). The class with a rate of change between 0.25 and 0.41 was the most dominant in the northern compartment. However, some plots in the southern part of the northern compartment showed a significant phenological change (from 0.41 to 0.58). whereas the rate of growth in the southern compartment was lower (from 0.08 to 0.41) than in the northern compartment.

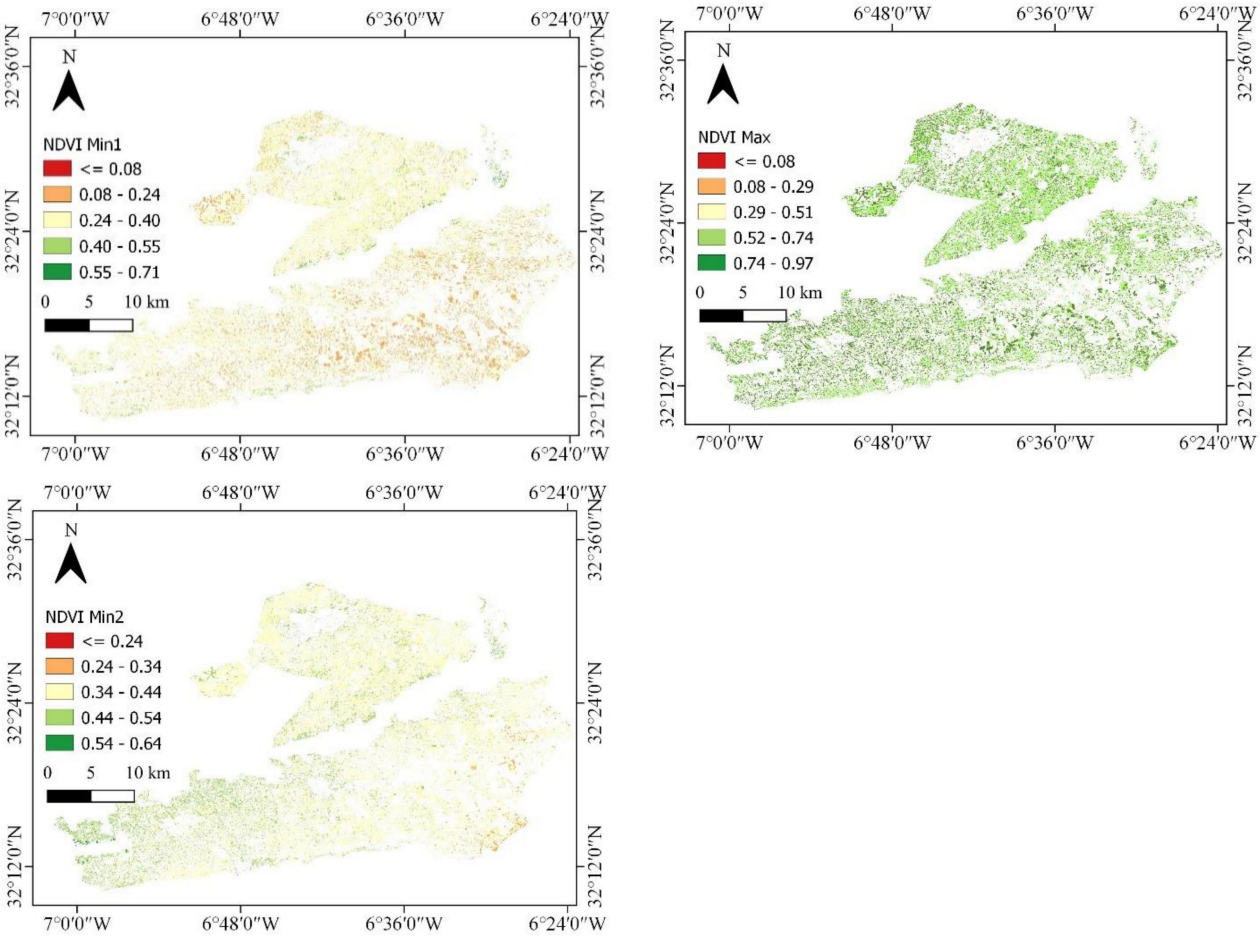

Figure 12. $NDVI_{Min1}$, $NDVI_{Max}$, and $NDVI_{Min2}$ for the TIP region.

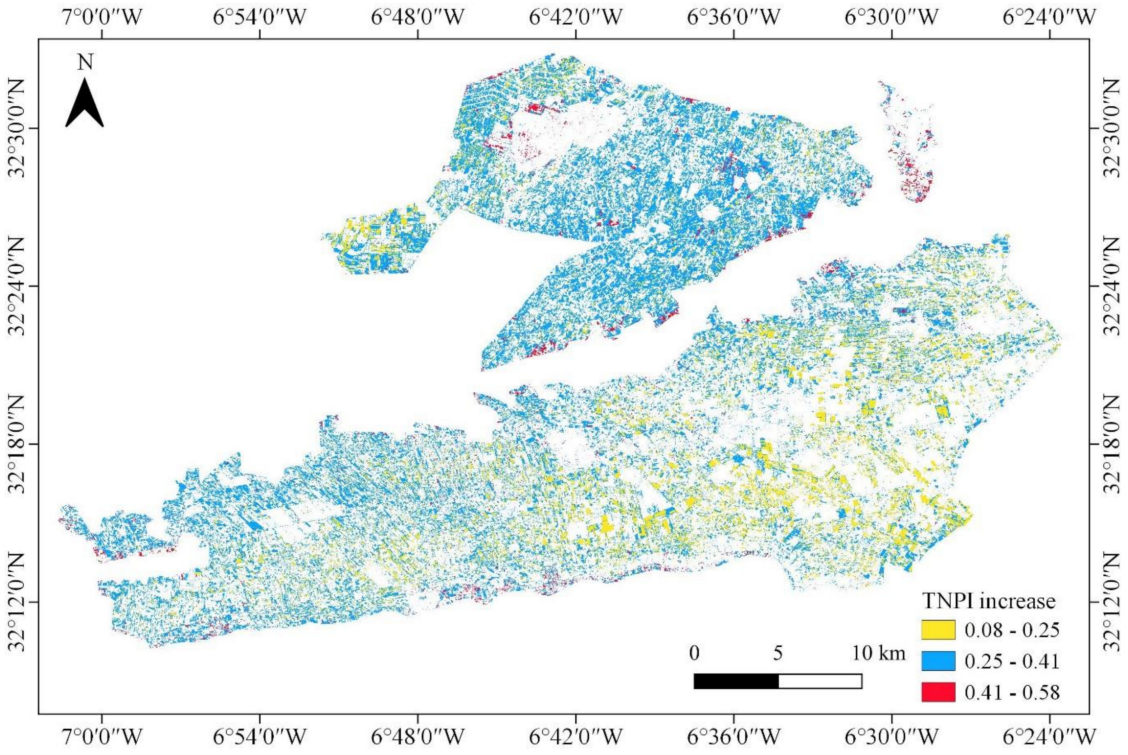

Figure 13. Crop growth increase based on TNPI during two phenological phases (germination and heading).

The TNPI decrease quantifies the change between the heading and harvesting period. The TNPI decrease values achieved ranged from 0.58 to 1 (Figure 13). The plots in the western part of the southern compartment showed the greatest rate of change (from 0.84 to 1). When compared to the phase between germination and heading, the phase between heading and harvesting showed a significant difference. Greater TNPI increase values indicate improved crop growth and vitality, while higher TNPI decrease values indicate a rapid decline in NDVI values at maturity stages.

5.7. Extrapolation of the Phenology Estimation Model from the Field to the Region Scale

The most accurate optical and SAR models (Model 3, with an R^2 = 0.70 and Model 7, with an R^2 = 0.84) were selected and applied for upscaling and mapping the five phonological stages of wheat across the full research area according to the phenological calendar of wheat (Figure 2). The extrapolated models produced ten phenological maps that were classified into five classes: 0–1: germination, 1–2: tillering, 2–3: jointing, 3–4: heading, 4–5: maturity. For this reason, a color bar was generated in which a unique color code is matched with each phenological stage. For example, since the first recorded germination date at the field scale was 330 DOY, the same color code was applied to all plots that experienced germination between 330 DOY and 337 DOY, and so on. This allowed a better comparison and statical analysis afterwards. Figures 14 and 15 show the produced maps.

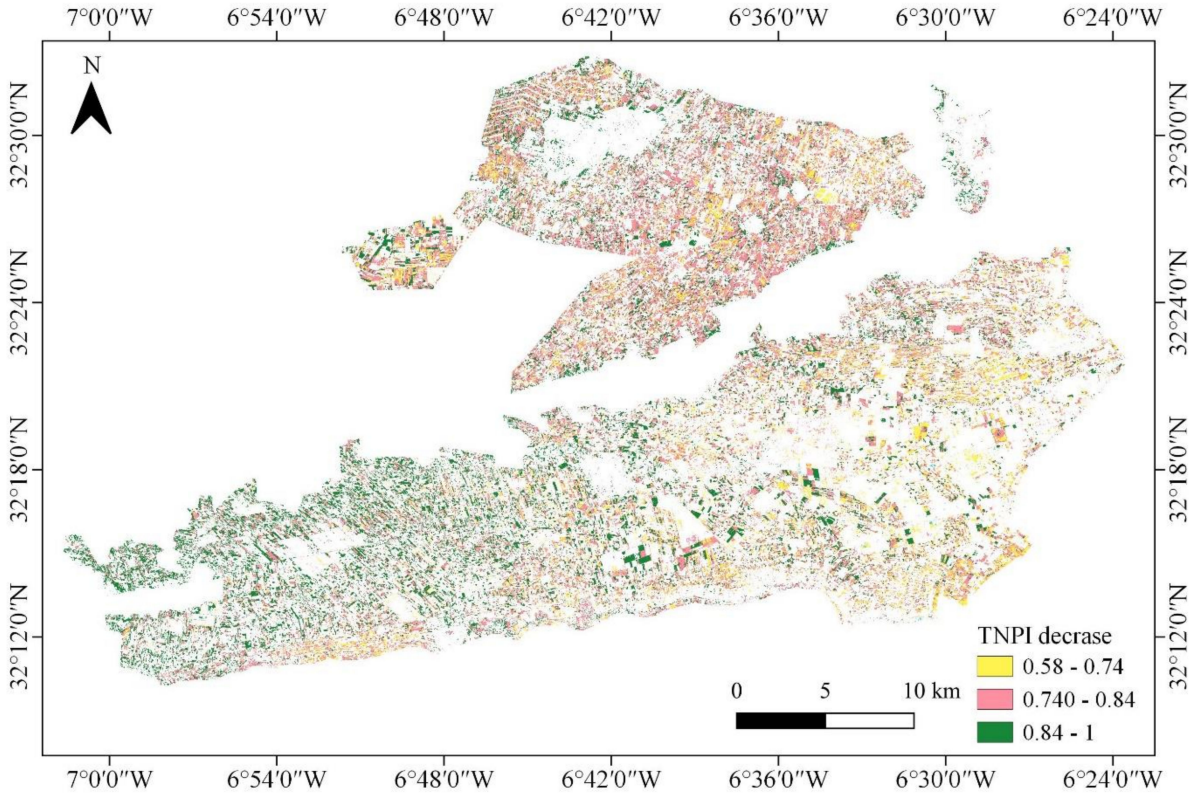

Figure 14. Crop growth increase based on TNPI during two phenological phases (heading and maturity).

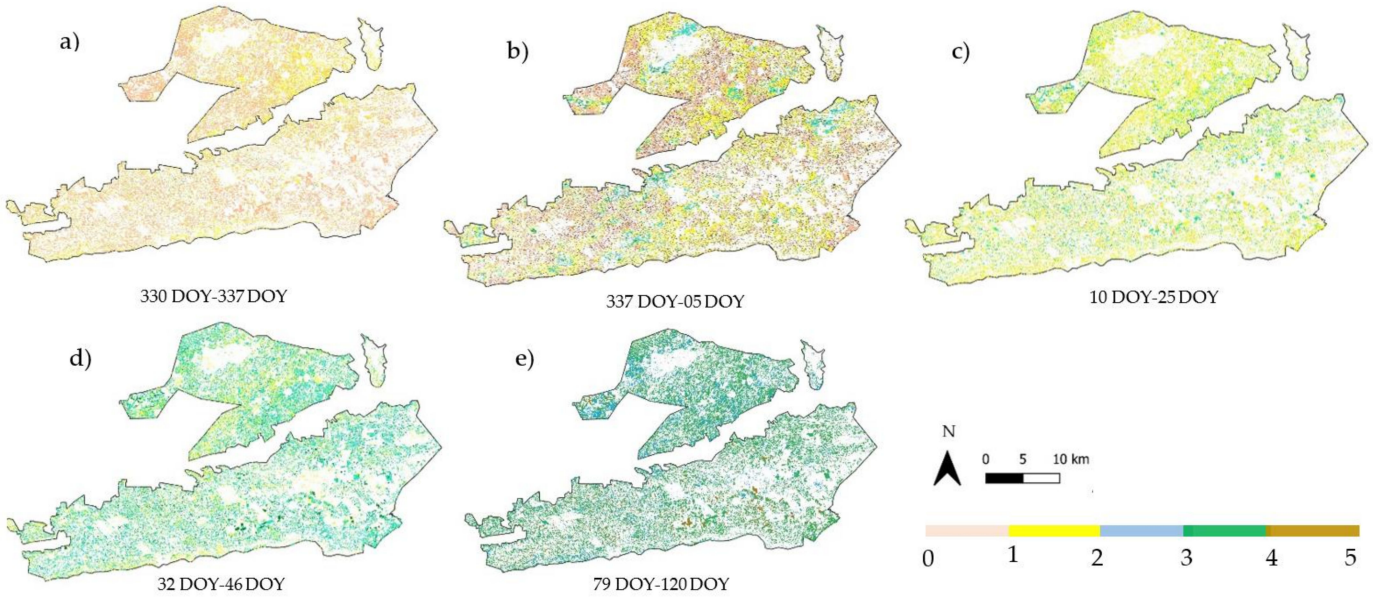

Figure 15. Maps of the five phenological stages of wheat for the TIP region deduced from Sentinel-2 (Model 3). The color bar represents the 0–1: germination, 1–2: tillering, 2–3: jointing, 3–4: heading, 4–5: maturity phases.

According to Figures 15 and 16 and Table 7, during germination (330 DOY–337 DOY), Sentinel-2 had the potential to predict the germination phase and around 40% of the plots completed this stage. From Figure 15, however, this stage was less discriminated when using the Sentinel-1 model, with only 28% of the plots being assigned to germination. As for the tillering and jointing stages (337 DOY–05 DOY and 10 DOY–25 DOY), Sentinel-2 had

the ability to predict these phases. In terms of tillering, around 40% of the plots completed this stage. In terms of jointing, around 69% of the plots completed this stage.

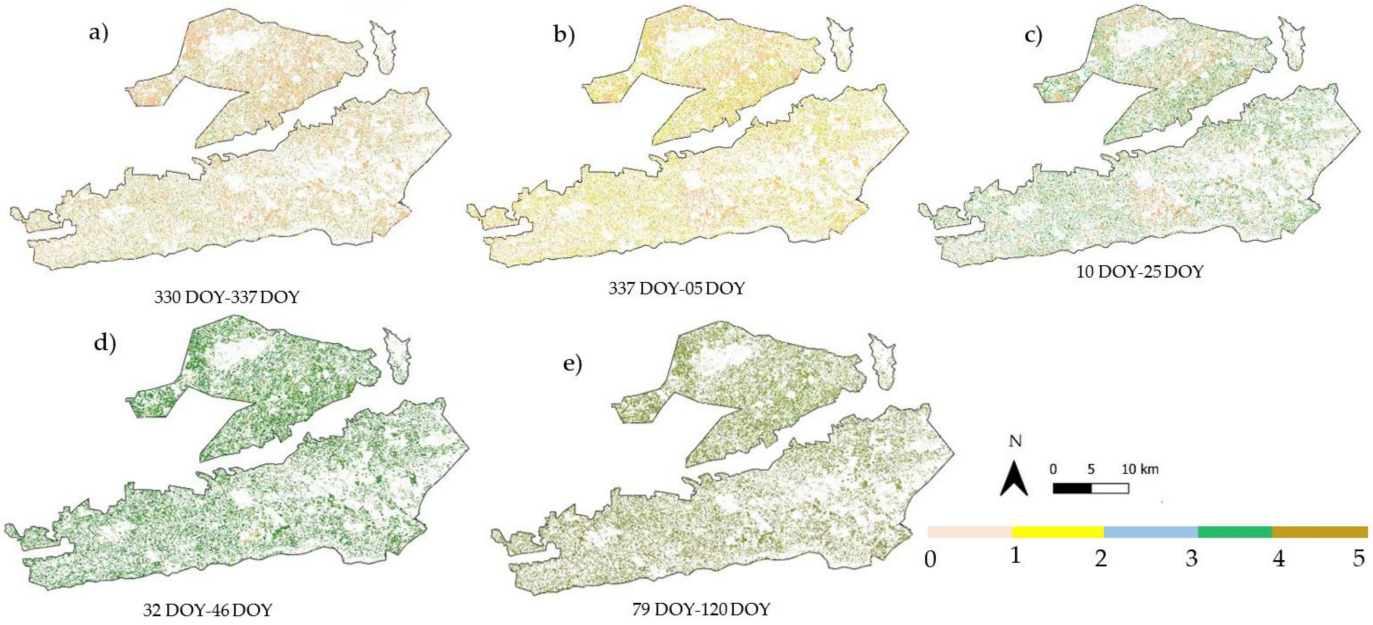

Figure 16. Maps of the five phenological stages of wheat for the TIP region deduced from Sentinel-1 (Model 7). The color bar represents the 0–1: germination, 1–2: tillering, 2–3: jointing, 3–4: heading, 4–5: maturity phases.

Table 7. Estimated area of wheat phenological stages in the TIP region using Sentinel-1 (Model 7) and Sentinel-2 (Model 3): 0–1: germination, 1–2: tillering, 2–3: jointing, 3–4: heading, 4–5: maturity.

Phenological Stage	Phenological Model	0–1		1–2		2–3		3–4		4–5	
0–1	Sentinel-1 (Model 7)	13,391 ha	28%	13,472 ha	29%	8817 ha	18%	6222 ha	13%	4720ha	10%
	Sentinel-2 (Model 3)	18,737 ha	40%	1458 ha	3%	22,494 ha	48%	3387 ha	7%	485 ha	1%
1–2	Sentinel-1 (Model 7)	16,499 ha	42%	11,419 ha	25%	9491 ha	20%	4790 ha	10%	1363 ha	3%
	Sentinel-2 (Model 3)	189 ha	0.4%	18665 ha	40%	26,383 ha	57%	1205 ha	2.5%	46,561 ha	0.2%
2–3	Sentinel-1 (Model 7)	11,730 ha	25%	10,085 ha	21%	11,693 ha	25%	8631ha	18%	4423 ha	9.5%
	Sentinel-2 (Model 3)	0 ha	0%	4881 ha	10.5%	32,003 ha	69%	9131 ha	20%	545 ha	1%
3–4	Sentinel-1 (Model 7))	1358 ha	3%	3344 ha	7%	9905 ha	21%	16,887 ha	36%	15,063 ha	32%
	Sentinel-2 (Model 3)	0 ha	0%	329 ha	0.1%	14,616 ha	31%	28,609 ha	61%	3008 ha	6.5%
4–5	Sentinel-1 (Model 7)	1345 ha	2.9%	3185 ha	6.84%	8604 ha	18%	15,942 ha	34%	17,486 ha	37.5%
	Sentinel-2 (Model 3)	0 ha	0%	247 ha	0.5%	34,714 ha	74%	11,462 ha	25%	139 ha	0.2%

However, during the heading and maturity stages (32 DOY–46 DOY and 79 DOY–120 DOY), Sentinel-1 was more efficient in predicting these stages, with around 36% of the plots achieving closed heading and 37.5% of the plots completed maturity. During these periods, Model 7, deduced from Sentinel-1, was not accurate in the discrimination between these phases, with about 36% of the plots having ended heading and 37.5% having completed maturity. Although, during these periods, Model 3, derived from Sentinel-2, was not accurate in discriminating between these stages. In terms of heading, 60% of the plots reached this stage, and 6.5% of plots reached maturity, which shows that the occupation attributed to heading exceeds its typical distribution, which results in a low accuracy in terms of predicting the ultimate phase of maturity.

6. Discussion

This research paves the way for a method to monitor the temporal behavior of wheat in the TIP region using Sentinel-1, Sentinel-2, and GEE cloud computing. To construct a phenological estimation model and extrapolate it from layers to the entire region, this work examined seven remote sensing indices and the computational capacity of GEE.

6.1. Sentinel-1 and Sentinel-2 Temporal Behavior

This study revealed that the spectral-temporal profile of wheat crops was consistent with those noticed by Veloso et al. [44], with decreasing values in the Red (B4) and SWIR (B11, B12) bands and increasing values in the NIR (B8, B8A) bands and red-edge bands (B6, B7) during the growing season of wheat. The signal variances were highest in the red-edge and NIR bands, while they were lowest in the RGB bands. The NDVI, EVI, WDVI, and S2REP values varied depending on the crop calendar recorded in the field (Figure 2). They all increase when the chlorophyll content was saturated at the tillering phase, while they all decreased at maturity, as the plant color changes and dries. The detailed analysis of these profiles allowed for the identification of the dates for tillering, jointing, heading, maturity as well as germination and harvesting. In the Bekaa plain of Lebanon, Nasrallah et al. [2] also discriminated the germination, heading, and soft dough phonological stages of wheat by analyzing the NDVI profile.

In this research, 20 Sentinel-2 images were acquired, as compared to 36 Sentinel-1 images within the same phonological growth period. The majority of the variability in the backscattering profiles can be physically understood by variations in the physical characteristics of plants [14]. This variability was adjusted by the VH–VV profile, which also provided a more accurate description of the phenological stages (Figure 7).

The phenological stages of wheat crops were also successfully discriminated from the scatterplot of the field samples of the wheat plots in a space including the NDVI and EVI, NDVI and WDVI, and NDVI and S2REP values, while these stages were not discriminated by the combination of VH, VV, and VH–VV polarization.

The Sentinel-1 and Sentinel-2 dense time series data were also used to produce a wheat map of the entire TIP region by generating the RF classifier, with an overall accuracy of %. From this map, a detailed investigation of the NDVI profile obtained was generated by extracting the TNPI increase and TNPI decrease. The achieved TNPI increase values revealed that the change between the germination and heading stages ranged from 0.08 to 0.58, representing an intermediate rate of change between these stages. The obtained TNPI decrease values ranged from 0.58 to 1, showing an important rate of change between the heading and harvesting periods. A higher increase in the TNPI value means improved crop growth and vitality, whereas a higher decrease in the value indicates a rapid decline in NDVI values at maturity. Similarly, Vaghela et al. [1] examined the phenological growth stages of wheat by computing the Temporal Normalized Phenology Index (TNPI) of growth stages.

6.2. Phenology Estimation Model

To quantitatively extract the phenological stages of wheat using Sentinel-1 and Sentinel-2 data, the seven optical and radar remote sensing indices were evaluated to develop an accurate phenology estimation model using the LR technique. The models created with WDVI as the independent variable were found to be the most accurate in predicting the phenological stages (R^2 = 0.76, RMSE = 0.77, nRMSE = 26%) when using Sentinel-2. In the case of Sentinel-1, the greatest phenological estimation model was the one that uses the VH–VV difference polarization (R^2 = 0.84, RMSE = 0.56, nRMSE = 18%).

These models were extrapolated at the regional scale. A statical analysis of results obtained from model 3 and model 7 at the regional scale showed that model 3 deduced from Sentienl-2 was preferred in the prediction of the germination, tillering, and jointing phases, while model 7 deduced from Sentinel-1 was superior in the prediction of the heading and maturity stages. Audrey et al. [16] deduced that the SAR signal is affected by the geometry and wetness of the examined wheat and rapeseed targets, while the optical signal is sensitive to their physiology. Thus, this study revealed that the phases from germination to jointing were better discriminated by the physiology of the wheat field rather than its structure. From heading to maturity, the structure of the wheat became rigid and drier, and, as a result, these phases were better identified with Sentinel-1 remote sensing indices.

Almost 40% of the plots in TIP region achieved germination throughout the period between 25 November 2020 (330 DOY) and 2 December 2020 (337 DOY) (Figure 14, Table 7). Given that the wheat plots were primarily planted on the ten last day of November, and that the germination of wheat seeds begins 5–7 days after planting and lasted for 7 days, this founding would appear to be reasonable and acceptable.

Regarding the tillering time (Figure 14), the estimated stage revealed that between December 2 (337 DOY) and January 05 (05 DOY), 2020/2021, 40% of the wheat plots (Table 7) experienced tillering. This area is a typical tillering period in the relevant location (Tadla Irrigated Perimeter).

The third mapped phenological phase after tillering was the jointing phase. By looking at Figure 14 and Table 7, around 69% of wheat plots completed jointing between 10 January (10 DOY) and 25 January 2021 (25 DOY).

The fourth mapped phenological period after jointing was the heading phase. By analyzing Figure 15 and Table 7, around 36% of wheat plots experienced heading between 01 February (32 DOY) and 15 March (46 DOY), 2021. As for the maturity season, in the TIP region, maturity happened between the ten last days of March (79 DOY) and the ten last days of April (120 DOY). Harvesting can be carried out from the 1st week of March when the crop has reached physiological maturity.

Furthermore, these results revealed that the phonological phases in the TIP region are mutually dependent. Wheat plots that experienced early germination reached the tillering, jointing, heading, and maturity stages earlier than those which achieved late germination. Table 8 presents an overview of recent work results on the monitoring of the phenological stages of wheat using Sentinel-1 and Sentinel-2 remote sensing data.

Table 8. Overview of recent works results on the monitoring of the phenological stages of wheat using Sentinel-1 and Sentinel-2 remote sensing data.

Author	Year	Problem Definition	Targeted Crop	Dataset	Model/Tools	Score
Ali Nasrallah et al. [2]	2019	Monitoring and mapping wheat phenology	Wheat	Sentinel-1 time series	Smoothing and fitting the temporal series with Gaussian functions	RMSE = 2.9–5.5 days
Audrey et al. [16]	2020	Prediction of phenological stages	Wheat and rapeseed	Sentinel-1 and Sentinel-2 time series	-Analysis of spectral temporal profiles -Incremental approach for estimating the remote sensing indices contribution to the classification of principal and secondary phenological stages.	Mean kappa = 0.53–0.82 (wheat), 0.74–0.92 (rapeseed)
Katharina et al. [15]	2021	Detection of phenological development stages	Wheat	Sentinel-1 and Sentinel-2 time series	The sensitivity of remote sensing features to phenological development	<5 days
Linlin et al. [45]	2014	Prediction of phenological stages	Wheat	SPOT-VEGETATION data	Double-Gaussian model	R^2 = 0.53

7. Conclusions

- The use of remote sensing indices and cloud computing is still in its infancy when it comes to agriculture policy and practices in the Tadla Irrigated Perimeter region. This was the first time a Linear Regression model (LR) derived from remote sensing indices was developed to estimate crop production in the TIP. More specifically, it was found that the dense time series of Sentinel-2 (NDVI, EVI, WDVI, and S2REP) and Sentinel-1 (VH, VV, and VH–VV) were able to precisely identify phenological stages, i.e., germination, tillering, jointing heading, maturity, and harvesting, with the support of rainfall temperature data as well as a ground data penological survey. Thus, a more accurate monitoring of the phenological development of wheat was achieved.
- Despite the phenological similarity between phenological phases, it was possible to identify stages in which these phases can be differentiated using scatter plots of field samples of wheat plots in a space comprising the vegetation indices and the backscattering coefficient.
- The suggested TNPI temporal index provided a better level of comprehension in terms of phenological changes at two phases than utilizing single NDVI data, resulting in a reduction in the amount of time series data to be analyzed.
- Google Earth Engine cloud computing should be further explored, as it provided very good performance in terms of accessing remote sensing products and reducing the processing time, computation, and automation.
- The optimal models for predicting phenological stages were generated from the WDVI and VH–VV remote sensing indices, resulting in an R2 equal to 0.70 from germination to jointing and an R2 equal to 0.84 from heading to maturity
- Many prospective investigations related to crop monitoring based on Sentinel-1 and Sentinel-2, such as dynamic crop mapping and biophysical parameter estimates, will benefit from a deeper knowledge of optical and SAR temporal behaviors in real-time under varying agricultural practices and environmental conditions.

Author Contributions: Conceptualization, H.S.E.I. and A.E.H.; methodology, H.S.E.I. and A.E.H.; software, H.S.E.I. and J.P.; validation, A.E.H.; formal analysis, H.S.E.I.; investigation, H.S.E.I.; resources, H.S.E.I. and A.E.H.; data curation, H.S.E.I., A.E.H., and J.P.; writing—original draft preparation, H.S.E.I.; writing—review and editing, A.E.H.; visualization, H.S.E.I.; supervision, A.E.H.; project administration, H.S.E.I.; funding acquisition, H.S.E.I. All authors have read and agreed to the published version of the manuscript.

Funding: This research received no external funding.

Institutional Review Board Statement: Not applicable.

Informed Consent Statement: Informed consent was obtained from all subjects involved in the study.

Data Availability Statement: All results and data are included in the supporting files, which have been archived online via Zenodo: https://doi.org/10.5281/zenodo.5122842.

Acknowledgments: We would like to acknowledge the Google Earth Engine platform (GEE), powered by Google's cloud infrastructure, for providing public data archives and a rapid and accurate process. We gratefully acknowledge the anonymous referees for their contribution to the paper via their consistent revisions and remarks.

Conflicts of Interest: The authors declare no conflict of interest.

References

1. Vaghela, B.N.; Solanki, H.A.; Kalubarme, M.H. Winter wheat growth assessment using Temporal Normalized Phenology Index (TNPI) in Bhuj Taluka, Gujarat State, India. *Remote Sens. Appl. Soc. Environ.* **2020**, *20*, 100422. [CrossRef]
2. Nasrallah, A.; Baghdadi, N.; El Hajj, M.; Darwish, T.; Belhouchette, H.; Faour, G.; Darwich, S.; Mhawej, M. Sentinel-1 data for winter wheat phenology monitoring and mapping. *Remote Sens.* **2019**, *11*, 2228. [CrossRef]
3. El Harti, A.; Lhissou, R.; Chokmani, K.; Ouzemou, J.E.; Hassouna, M.; Bachaoui, E.M.; El Ghmari, A. Spatiotemporal monitoring of soil salinization in irrigated Tadla Plain (Morocco) using satellite spectral indices. *Int. J. Appl. Earth Obs. Geoinf.* **2016**, *50*, 64–73. [CrossRef]
4. Ouzemou, J.E.; El Harti, A.; Lhissou, R.; El Moujahid, A.; Bouch, N.; El Ouazzani, R.; Bachaoui, E.M.; El Ghmari, A. Crop type mapping from pansharpened Landsat 8 NDVI data: A case of a highly fragmented and intensive agricultural system. *Remote Sens. Appl. Soc. Environ.* **2018**, *11*, 94–103. [CrossRef]
5. Htitiou, A.; Boudhar, A.; Lebrini, Y.; Hadria, R.; Lionboui, H.; Benabdelouahab, T. A comparative analysis of different phenological information retrieved from Sentinel-2 time series images to improve crop classification: A machine learning approach. *Geocarto Int* **2022**, *37*, 1426–1449. [CrossRef]
6. Khellouk, R.; Barakat, A.; Boudhar, A.; Hadria, R.; Lionboui, H.; El Jazouli, A.; Rais, J.; El Baghdadi, M.; Benabdelouahab, T. Spatiotemporal monitoring of surface soil moisture using optical remote sensing data: A case study in a semi-arid area. *J. Spat. Sci* **2020**, *65*, 481–499. [CrossRef]
7. Idol, T.; Haack, B.; Mahabir, R. An evaluation of Radarsat-2 individual and combined image dates for land use/cover mapping. *Geocarto Int.* **2016**, *31*, 1108–1122. [CrossRef]
8. Liu, C.-A.; Chen, Z.-X.; Shao, Y.; Chen, J.-S.; Hasi, T.; Pan, H.-Z. Research advances of SAR remote sensing for agriculture applications: A review. *J. Integr. Agric.* **2019**, *18*, 506–525. [CrossRef]
9. Van Tricht, K.; Gobin, A.; Gilliams, S.; Piccard, I. Synergistic use of radar sentinel-1 and optical sentinel-2 imagery for crop mapping: A case study for Belgium. *Remote Sens.* **2018**, *10*, 1642. [CrossRef]
10. Albert, G.; Ammar, S. Application of random forest classification and remotely sensed data in geological mapping on the Jebel Meloussi area (Tunisia). *Arab. J. Geosci.* **2021**, *14*, 2240. [CrossRef]
11. Nasirzadehdizaji, R.; Cakir, Z.; Balik Sanli, F.; Abdikan, S.; Pepe, A.; Calò, F. Sentinel-1 interferometric coherence and backscattering analysis for crop monitoring. *Comput. Electron. Agric.* **2021**, *185*, 106118. [CrossRef]
12. Panchal, J.; Shukla, S.H.; Kalubarme, M. Analysis of Optimum Growth Stages for Winter Crop Separability using Multi-Temporal NDVI Profiles in Vijapur Taluka, Gujarat State. *Int. J. Environ. Geoinformatics* **2021**, *8*, 135–143. [CrossRef]
13. Khare, S.; Ghosh, S.K.; Latifi, H.; Vijay, S. Seasonal-based analysis of vegetation response to environmental variables in the mountainous forests of Western Himalaya using Landsat 8 data. *Int. J. Remote Sens.* **2017**, *38*, 4418–4442. [CrossRef]
14. Veloso, A.; Mermoz, S.; Bouvet, A.; Le Toan, T.; Planells, M.; Dejoux, J.F.; Ceschia, E. Understanding the temporal behavior of crops using Sentinel-1 and Sentinel-2-like data for agricultural applications. *Remote Sens. Environ.* **2017**, *199*, 415–426. [CrossRef]
15. Harfenmeister, K.; Itzerott, S.; Weltzien, C.; Spengler, D. Detecting phenological development of winter wheat and winter barley using time series of sentinel-1 and sentinel-2. *Remote Sens.* **2021**, *13*, 5036. [CrossRef]
16. Mercier, A.; Betbeder, J.; Baudry, J.; Le Roux, V.; Spicher, F.; Lacoux, J.; Roger, D.; Hubert-Moy, L. Evaluation of Sentinel-1 & 2 time series for predicting wheat and rapeseed phenological stages. *ISPRS J. Photogramm. Remote Sens.* **2020**, *163*, 231–256. [CrossRef]
17. Ren, J.; Chen, Z.; Zhou, Q.; Tang, H. Regional yield estimation for winter wheat with MODIS-NDVI data in Shandong, China. *Int. J Appl. Earth Obs. Geoinf.* **2008**, *10*, 403–413. [CrossRef]

18. Mehdaoui, R.; Anane, M. Exploitation of the red-edge bands of Sentinel 2 to improve the estimation of durum wheat yield in Grombalia region (Northeastern Tunisia), 2020, 41:23, 8986–9008. *Int. J. Remote Sens.* **2020**, *41*, 8986–9008. [CrossRef]
19. Becker-Reshef, I.; Vermote, E.; Lindeman, M.; Justice, C. A generalized regression-based model for forecasting winter wheat yields in Kansas and Ukraine using MODIS data. *Remote Sens. Environ.* **2010**, *114*, 1312–1323. [CrossRef]
20. Zhu, B.; Chen, S.; Cao, Y.; Xu, Z.; Yu, Y.; Han, C. A regional maize yield hierarchical linear model combining landsat 8 vegetative indices and meteorological data: Case study in Jilin Province. *Remote Sens.* **2021**, *13*, 356. [CrossRef]
21. Roznik, M.; Boyd, M.; Porth, L. Improving crop yield estimation by applying higher resolution satellite NDVI imagery and high-resolution cropland masks. *Remote Sens. Appl. Soc. Environ.* **2022**, *25*, 100693. [CrossRef]
22. Tuvdendorj, B.; Wu, B.; Zeng, H.; Batdelger, G.; Nanzad, L. Determination of appropriate remote sensing indices for spring wheat yield estimation in Mongolia. *Remote Sens.* **2019**, *11*, 2568. [CrossRef]
23. Spoto, F.; Martimort, P.; Drusch, M. Sentinel-2: ESA's optical high-resolution mission for GMES operational services. *Remote Sens. Environ.* **2020**, *120*, 25–36.
24. Meng, Q.; Cooke, W.H.; Rodgers, J. Derivation of 16-day time-series NDVI data for environmental studies using a data assimilation approach. *GIScience Remote Sens.* **2013**, *50*, 500–514. [CrossRef]
25. Borgogno-Mondino, E.; De Palma, L.; Novello, V. Investigating Sentinel 2 Multispectral Imagery Efficiency in Describing Spectral Response of Vineyards Covered with Plastic Sheets. *Agronomy* **2020**, *10*, 1909. [CrossRef]
26. Tufail, R.; Ahmad, A.; Javed, M.A.; Ahmad, S.R. A machine learning approach for accurate crop type mapping using combined SAR and optical time series data. *Adv. Space Res.* **2022**, *69*, 331–346. [CrossRef]
27. Seguin, B.; Courault, D.; Guérif, M. Satellite thermal infrared data applications in agricultural meteorology. *Adv. Space Res.* **1993**, *13*, 207–217. [CrossRef]
28. Kouadio, L.; Newlands, N.K.; Davidson, A.; Zhang, Y.; Chipanshi, A. Assessing the performance of MODIS NDVI and EVI for seasonal crop yield forecasting at the ecodistrict scale. *Remote Sens.* **2014**, *6*, 10193–10214. [CrossRef]
29. HLiu, H.Q.; Huete, A. Feedback based modification of the NDVI to minimize canopy background and atmospheric noise. *IEEE Trans. Geosci. Remote Sens.* **1995**, *33*, 457–465. [CrossRef]
30. Clevers, J.G.P.W. Application of a weighted infrared-red vegetation index for estimating leaf Area Index by Correcting for Soil Moisture. *Remote Sens. Environ.* **1989**, *29*, 25–37. [CrossRef]
31. Ghosh, K.; Samui, R.P.; Narayanan, P.S. Reflectance characteristics of maize and application of vegetation indices for estimation of leaf area index. *Mausam* **2003**, *54*, 901–908. [CrossRef]
32. You, Q. Determining paddy field spatiotemporal distribution and temperature influence using remote sensing in Songnen Plain, Northeastern China. *Arab. J. Geosci.* **2020**, *13*, 1075. [CrossRef]
33. Gómez-Giráldez, P.J.; Pérez-Palazón, M.J.; Polo, M.J.; González-Dugo, M.P. Monitoring grass phenology and hydrological dynamics of an oak-grass savanna ecosystem using sentinel-2 and terrestrial photography. *Remote Sens.* **2020**, *12*, 600. [CrossRef]
34. Imran, A.B.; Khan, K.; Ali, N.; Ahmad, N.; Ali, A.; Shah, K. Narrow band based and broadband derived vegetation indices using Sentinel-2 Imagery to estimate vegetation biomass. *Glob. J. Environ. Sci. Manag.* **2020**, *6*, 97–108. [CrossRef]
35. Guyot, G.; Baret, F. Utilisation de la haute resolution spectrale pour suivre l'etat des couverts vegetaux. *J. Chem. Inf. Model.* **1988**, *53*, 1689–1699.
36. Niculescu, S.; Ali, H.T.O.; Billey, A. Random forest classification using Sentinel-1 and Sentinel-2 series for vegetation monitoring in the Pays de Brest (France). *Remote Sens. Agric. Ecosyst. Hydrol.* **2018**, *10783*, 1078305. [CrossRef]
37. Rouse, J.H. *Monitoring Vegetation Systems in the Great Plains with ERTS*; NASA SP-351; NASA: Washington, DC, USA, 1973; pp. 309–317.
38. Huete, A.D. Overview of the radiometric and biophysical performance of the MODIS vegetation indices. *Remote Sens. Environ.* **2002**, *83*, 195–213. [CrossRef]
39. Breiman, L. Statistical Modeling: The Two Cultures (with comments and a rejoinder by the author). *Stat. Sci.* **2021**, *16*, 199–231. [CrossRef]
40. Adam, E.; Mutanga, O.; Odindi, J.; Abdel-Rahman, E.M. Land-use/cover classification in a heterogeneous coastal landscape using RapidEye imagery: Evaluating the performance of random forest and support vector machines classifiers. *Int. J. Remote Sens.* **2014**, *35*, 3440–3458. [CrossRef]
41. Shelestov, A.; Lavreniuk, M.; Kussul, N.; Novikov, A.; Skakun, S. Exploring Google earth engine platform for big data processing: Classification of multi-temporal satellite imagery for crop mapping. *Front. Earth Sci.* **2017**, *5*, 1–10. [CrossRef]
42. Luo, C.; Liu, H.-J.; Lu, L.-P.; Liu, Z.-R.; Kong, F.-C.; Zhang, X.-L. Monthly composites from Sentinel-1 and Sentinel-2 images for regional major crop mapping with Google Earth Engine. *J. Integr. Agric.* **2021**, *20*, 1944–1957. [CrossRef]
43. Aduvukha, G.R.; Abdel-Rahman, E.M.; Sichangi, A.W.; Makokha, G.O.; Landmann, T.; Mudereri, B.T.; Tonnang, H.E.Z.; Dubois, T. Cropping Pattern Mapping in an Agro-Natural Heterogeneous Landscape Using Sentinel-2 and Sentinel-1 Satellite Datasets. *Agriculture* **2021**, *11*, 530. [CrossRef]
44. Gazzinelli, A.; Oliveira-Prado, R.; Matoso, L.F.; Veloso, B.M.; Andrade, G.; Kloos, H.; Bethony, J.M.; Assunção, R.M.; Correa-Oliveira, R. Schistosoma mansoni reinfection: Analysis of risk factors by classification and regression tree (CART) modeling. *PLoS ONE* **2017**, *12*, e0182197. [CrossRef]
45. Lu, L.; Wang, C.; Guo, H.; Li, Q. Detecting winter wheat phenology with SPOT-VEGETATION data in the North China Plain. *Geocarto Int.* **2014**, *29*, 244–255. [CrossRef]